ERK1/2 signalling dynamics promote neural differentiation by regulating the polycomb repressive complex

Claudia I. Semprich, Vicki Metzis[1], Harshil Patel[2], James Briscoe[1] and Kate G. Storey*

Division of Cell & Developmental Biology
School of Life Sciences, University of Dundee,
Dow Street, DD1 5EH, Scotland, UK

[1]The Francis Crick Institute, [2]Bioinformatics and Biostatistics
1 Midland Road, London, NW1 1AT, UK

* Correspondence: k.g.storey@dundee.ac.uk

Running title: ERK1/2 promotes differentiation via PRC

Key words: Neural differentiation; neural induction; mouse embryo; caudal lateral epiblast; human embryonic stem cells; neuromesodermal progenitors; FGF signalling; ERK1/2 signalling; polycomb repressive complex ; ATAC-seq;

Abstract

Fibroblast Growth Factor (FGF) is a neural inducer in many vertebrate embryos, but how it regulates chromatin organization to coordinate the activation of neural genes is unclear. Moreover, for differentiation to progress FGF signalling has to decline. Why this signalling dynamic is required has not been determined. Here we show that dephosphorylation of the FGF effector kinase ERK1/2 rapidly increases chromatin accessibility at neural genes in mouse embryos and, using ATAC-seq in human embryonic stem cell derived spinal cord precursors, we demonstrate that this occurs across hundreds of neural genes. Importantly, while Erk1/2 inhibition induces precocious neural gene transcription, this step involves dissociation of the polycomb repressive complex from gene loci and takes places independently of subsequent loss of the repressive histone mark H3K27me3 and transcriptional onset. We find that loss of ERK1/2 activity but not its occupancy at neural genes is critical for this mechanism. Moreover, transient ERK1/2 inhibition is sufficient for polycomb protein dissociation and this is not reversed on resumption of ERK1/2 signalling. These data indicate that ERK1/2 signalling maintains polycomb repressive complexes at neural genes, that its decline coordinates their increased accessibility and that this is a directional molecular mechanism, which initiates the process of neural commitment. Furthermore, as the polycomb repressive complexes repress but also ready genes for transcription, these findings suggest that ERK1/2 promotion of these complexes is a rite of passage for subsequent differentiation.

Introduction

The identities of signals that induce particular cell fates are now well-established, but how such signalling regulates chromatin to coordinate the transcription of differentiation genes and so orchestrate engagement of a differentiation programme is not well understood. Fibroblast growth factor (FGF) signalling has been implicated in the acquisition of neural cell fate in many vertebrate embryos [1-7]; reviewed in [8] (although the timing of involvement varies between species and may reflect differences in induction of anterior and posterior regions [6, 9, 10]). Intriguingly, while FGF is required for neural induction in most of these contexts, its decline is also necessary for differentiation progression.

The requirement for transient FGF signalling to promote neural differentiation is particularly evident in the elongating embryonic body axis in which the spinal cord is generated progressively, as here there is a clear spatial separation of the temporal events of differentiation. FGF acts, along with Wnt signalling, in the caudal lateral epiblast (CLE)/node streak border (which later form the tailbud) to maintain a multipotent cell population known as neuromesodermal progenitors (NMP) which progressively gives rise to the spinal cord and paraxial mesoderm (Figure 1A) [11-15] reviewed in Henrique et al., 2015). Blocking FGF signalling in this cell population accelerates the onset of neural differentiation genes and ectopic maintenance of FGF inhibits this step [16-18]. During normal development differentiation onset is promoted by rising retinoid signalling, provided by adjacent paraxial mesoderm, which represses *Fgf8*, restricting it to the tail end (Figure 1A) [17-20] reviewed in [21]. These findings indicate that decline in FGF signalling promotes neural differentiation, however, little is known about the mechanism(s) by which such signalling dynamics mediate the coordinated activation of neural differentiation genes.

Importantly, as NMP progeny leave the CLE and embark on neural differentiation they experience loss of the FGF effector kinase ERK1/2/MAPK (hereafter referred to as ERK1/2) activity in both chick and mouse embryos [22, 23]. This suggests that ERK1/2 signalling dynamics may regulate onset of neural differentiation. The *in vitro* manipulation of embryonic stem (ES) cells has provided some insight into the

involvement of ERK1/2 signalling in this process. Rather than promoting differentiation however, inhibition of ERK1/2 activity in mouse ES cells supports pluripotency [24, 25] and exposure to FGF/ERK1/2 signalling appears here to be an initial step towards differentiation. In agreement with this, FGF is required for neural differentiation of mES cells [26-28] although the timing of this requirement differs between assays [29]. Importantly, however, only a short critical period of ERK1/2 signalling is required in mES cells for subsequent expression of neural genes [27], after which FGF inhibition then accelerates neural differentiation [27, 30, 31]. Moreover, in mouse epiblast stem cells (mEpiSC), which rely on FGF for self-renewal, prolonged FGF signaling abrogates neural differentiation [32]. Consistent with this in both mEpiSCs and human ES cells (which also depend on FGF for self-renewal), inhibition of FGF/ERK1/2 signalling promotes neural differentiation [30, 32]. These findings indicate that temporal control over FGF/ERK1/2 signalling is instrumental in the estabishment of neural identity from epiblast cell precursors.

A clue to the mechanism by which FGF regulates neural differentiation was revealed by analysis of chromatin organisation at key neural progenitor genes in the mouse embryo CLE [33]. This showed that FGF signalling promotes compaction at *Pax6* and further that inhibition of this pathway in *Raldh2* mutant embryos decompacted this locus, even in this retinoid deficient condition in which *Pax6* fails to be expressed [33]. This indicated that FGF regulation of chromatin organisation is molecularly distinct from the machinery that drives subsequent gene transcription, but left open the question of how FGF signalling modifies chromatin organisation. Potential targets for FGF include the polycomb repressive complexes 1 and 2 (PRC1 and 2), which are involved in the repression of differentiation genes in many contexts [34-40] reviewed in [41]. PRC2 is composed of core proteins Ezh2, Eed and Suz12, and via Ezh2 catalyses the methylation of histone 3 lysine 27 (H3K27me2/3) [42-45] and this is augmented in mES cells by the accessory protein, Jarid2 [46-50]. Methylation of H3K27 provides a docking site for PRC1, which in turn directs chromatin compaction and inhibits transcription from target gene loci [51-53] reviewed in [54]. Intriguingly, ERK1/2 inhibition in mES cells, while driving cells into a naïve pluripotent cell state leads to reduction in PRC2 at developmental genes [55-57]. This suggests a role for ERK1/2 signalling in the recruitment or maintenance of polycomb mediated repression. There is also evidence that this may

involve regulation by ERK1/2 protein association with PRC occupied chromatin in mES cells [56], although this appears not to be conserved in human ES cells [58].

Here we provide evidence in the caudal mouse embryo and in analogous human ES cell-derived spinal cord precursors, that inhibition of ERK1/2 activity rapidly increases chromatin accessibility at neural differentiation genes. We demonstrate that ERK1/2 dephosphorylation promotes precocious neural gene expression and that loss of PRCs is a molecularly distinct event that precedes transcription. We further show that it is loss of ERK activity, but not its association with chromatin, that leads to the disassociation of polycomb proteins from neural gene loci. Strikingly, this loss of PRCs requires only transient ERK1/2 inhibition and is not reversible upon resumption of ERK1/2 signalling. These findings reveal the succession of genome-wide, molecular mechanisms operating downstream of FGF/ERK1/2 signalling, that engage the neural differentiation programme.

Results

Chromatin compaction around neural differentiation gene *Pax6* in mouse embryos is ERK1/2 dependent

To determine whether ERK1/2 signalling regulates chromatin organisation at neural differentiation gene loci *in vivo*, we exposed whole mouse embryos (E8.5) to the small molecule MEK inhibitor PD184352 (MEKi) or vehicle only DMSO control for one hour (Figure 1B). The efficiency of ERK1/2 inhibition was determined by quantifying levels of phosphorylated ERK1/21/2 (42 and 44 kD) in whole protein extracts from MEKi and DMSO treated embryos (Figures 1C, C'). This regime was then used to measure chromatin compaction around the *Pax6* locus using Fluorescent *In Situ* Hybridisation (FISH) with fosmid probes hybridising either side of the locus [33] (Figure 1D). Chromatin compaction was assessed by measuring inter-probe distance in *Pax6* transcribing neural tube cells and in CLE cells where *Pax6* has yet to be expressed (Figures 1D', D''). In untreated embryos, the inter-probe distance was greater in neural tube than in CLE nuclei (Figures 1D', D''). Similar observations were made in the DMSO treated embryos (Figures 1D', D'') and these two control conditions were not significantly different, suggesting that DMSO did not alter chromatin organisation. By contrast, the *Pax6* locus was more open in CLE nuclei of MEKi treated embryos compared to both controls (Figures 1D', D''). This decompaction correlated with a 1.7 fold decrease in the number of base pairs per nm compared to controls. These findings indicate that ERK1/2 activity promotes chromatin compaction at this neural differentiation gene locus and that active ERK1/2 is acutely required for this action *in vivo*.

Figure 1 Rapid chromatin decompaction at the neural progenitor gene *Pax6* in the caudal lateral epiblast following ERK1/2 dephosphorylation in the developing mouse embryo. (A) E8.5 mouse embryo schematic, showing the caudal region and signalling pathways known to regulate neural differentiation, NT neural tube, CLE caudal lateral epiblast, RA retinoic acid, *RAR* retinoic acid receptor, FGF, fibroblast growth factor, *Raldh2* Retinaldehyde dehydrogenase 2; (B) Schematic of the hanging drop culture used to treat E8.5 mouse embryos with small molecule MEK inhibitor (MEKi, PD184352) or vehicle control DMSO for 1h; (C and C') Representative Western blot of embryo lysates probed with antibodies against total (panERK1/2) and phosphorylated ERK1/2 (dpERK1/2) and LiCOR quantification data (n = 3 independent experiments, error bar = SEM, * p= <0.05); (D) Position of fosmid probes flanking the *Pax6* locus (interprobe probe distance ca. 45kb); (D') representative examples of fosmid probes in individual NT and CLE nuclei (white dashed line) visualised with DAPI (blue) in each untreated condition, vehicle control (DMSO) and MEKi (in DMSO) treated; (D'') Inter-probe distance measured in > 50 nuclei in NT and CLE in each of three embryos in each condition (n= > 150 nuclei/condition/region, Mann Whitney - test/RankSum-test **** $p \leq 0.0001$); (E) Schematic showing caudal end explant (full tissue thickness taken) in E8.5 embryo; (E') Chromatin from three biological replicates, each consisting of 30 pooled explants, were interrogated for H3K27me3 levels at transcription start sites (TSS) of *Pax6*, known PRC target *HoxD11* and at control regions (see text) compared to IgG background. 3 biological replicates (circle, triangle and diamond) and average (bar) shown, error bar = SEM.

142 **Polycomb-mediated histone modification H3K27me3 marks the neural differentiation gene *Pax6 in vivo***
143 To determine whether the PRCs regulate chromatin compaction around the *Pax6* locus *in vivo*, we carried
144 out chromatin immunoprecipitations (ChIPs) for the PRC-mediated histone modification H3K27me3.
145 Mouse embryo microdissection was performed to enrich for the caudal region at E8.5 for ChIP-qPCR
146 (Figure 1E and see Methods). The *Pax6* transcription start site (TSS) was marked by high levels of
147 H3K27me3 indicative of polycomb activity and consistent with repression of this gene in the CLE (Figure
148 1E'). Similar levels were also detected at the known PRC target *HoxD11* [59-61], which is also not
149 expressed in the mouse CLE at E8.5 [62]. By contrast, known PRC targets transcribed in the CLE, *HoxA7*
150 and *HoxB1*, [63], exhibited minimal levels of H3K27me3 at their TSSs. This was similar to levels detected
151 at control intergenic region and house-keeping gene *GAPDH* indicative of a lack of polycomb activity at
152 these loci (Figure 1 E'). Together these data demonstrate that polycomb activity at target genes is
153 selective *in vivo*, and identify *Pax6* as a potential polycomb target. This raises the question of whether
154 ERK1/2 activity directs polycomb occupancy and chromatin compaction and thus determines the onset
155 of neural gene transcription.

156

157 ***PAX6* locus decompaction correlates with polycomb protein dissociation, H3K27me3 loss and**
158 **transcription onset in a human *in vitro* model of spinal cord differentiation**
159 To test this, we developed an *in vitro* system to study neural differentiation during the generation of the
160 spinal cord. We reasoned that the use of human ESCs, with the slower progression to neural progenitor
161 cell identity, would provide a better temporal resolution of mechanisms mediating neural differentiation.
162 To this end, we directed the differentiation of human ESCs towards spinal cord [13, 64] (Figure 2A). This
163 regime involved the generation of NMP-like cells on day 3 (NMP-L D3), characterised by the co-expression
164 of *BRA* and *SOX2* and their differentiation into *PAX6* expressing neural progenitors by day 8 (NP D8),
165 which also transcribed the known PRC target *HOXD11* (Figures B-B'''). More detailed analysis further
166 revealed low level onset of *PAX6* on D6, anticipating the robust expression detected on D8 (Figure 2B''').
167 We next asked whether changes in chromatin compaction at *Pax6* occur during human neural
168 differentiation *in vitro*, as we had observed in mouse *in vivo* (Figure 1D). FISH was carried out in NMP-L
169 (D3) and NPs (D8) cells and the distances between the *PAX6*-flanking probes were measured (Figures 2C-
170 C''). This revealed a significant increase in inter-probe distance in NPs compared to NMP-Ls (Figures 2C,
171 C'). This indicates that the regulation of chromatin compaction is a conserved mechanism operating
172 during neural differentiation, that can be examined and recapitulated *in vitro*.

173 **Figure 2 *In vitro* differentiation of human ESC-derived NMP-L cells to NPs reveals locus decompaction correlates**
174 **with dissociation of polycomb repressive complexes and transcriptional onset at *PAX6*.** (A) Schematic of
175 differentiation regime used to generate first NMP-like cells (NMP-L (D3)) and then spinal cord progenitors (NPs (D8))
176 from human ESCs (D1 = Day1); (B-B''') transcription levels of *BRA, SOX2, HOXD11* and *PAX6* assessed by RTqPCR in

177 undifferentiated cells (hESCs), NMP-Ls (D3) and NPs (D8) for *PAX6* additionally on day 5 (D5) and day 6 (D6) of
178 differentiation (n=3 independent experiments, error bars = SEM). (C-C'') FISH to assess chromatin compaction
179 around the *PAX6* locus in NMP-L and NP. 2 probes flanking the target locus (inter-probe distance ca. 51 kb) were
180 hybridised and labelling visualised in DAPI stained nuclei (blue, outlined with white dashed line). Inter-probe
181 distance measurements in >50 nuclei in NMP-Ls and NPs in 3 individual experiments (n= > 150 nuclei/cell type,
182 Mann Whitney - test/RankSum-test, *** $p \leq 0.001$). (D-D''') ChIP-qPCRs investigating polycomb repressive complex
183 occupancy (Ring1B/PRC1 and Jarid2/PRC2) and the histone modifications H3K27me3 and H3K4me3 in NMP-L and
184 NP cells (n = 3 independent experiments indicated with circles, triangles and diamonds, bar = average, error bar =
185 SEM, * $p \leq 0.01$, t test).

186 To elucidate how chromatin compaction is regulated at the *PAX6* locus, we interrogated PRC
187 occupancy over developmental time. PRC1/(Ring1B) and PRC2/(Jarid2) occupancy, along with H3K27me3
188 were analysed by ChIP-qPCR at *PAX6* and control loci in NMP-Ls and NPs. These analyses established the
189 presence of PRC proteins and H3K27me3 at the TSS and along the gene body of *PAX6* and at the TSS of
190 known PRC target *HOXD11* in NMP-L cells and importantly demonstrated reduced occupancy at *PAX6*
191 and *HOXD11* in NPs (while baseline detection in the gene desert region (*Gw10*) and the housekeeping
192 gene *GAPDH* remained unchanged) (Figures 2D-D''). Strikingly, analysis of the active histone modification
193 H3K4me3 revealed no change at the *HOXD11* or *PAX6* TSSs during neural differentiation (Figure 2D''').
194 This suggests that polycomb mediated repression is the major activity restricting *PAX6* gene expression
195 in the NMP-L cells, not the low levels of H3K4me3. Together these findings demonstrate that this site-
196 specific deposition of PRC is transient and that its removal is characteristic of the neural progenitor cell
197 state.

198 **Progressive global increase in neural gene accessibility during *in vitro* human differentiation**

199 While these data suggested that PRC loss is required for the onset of neural gene transcription, it
200 remained unclear whether this regulation of chromatin accessibility is specific for *PAX6* or reflects a
201 general mechanism that mediates onset of neural gene transcription. To address this we performed a
202 global analysis of the chromatin accessibility landscape in cells as they differentiated into NPs from the
203 NMPL cell state, using ATAC-seq [65]. This involved differentiation of NMPL (D3) cells (as in Figure 2A)
204 and sampling cell populations at intervals (D5, D6 and D8). Analysis of the chromatin configuration across
205 the *PAX6* locus revealed increased accessibility at multiple sites, some as early as D5 and most prominent
206 by D6 (Figure 3A), including one region described as an intragenic *PAX6* enhancer region [66] (red box
207 Figure 3A). These early increases in chromatin accessibility correlated with decline in PRC protein
208 occupancy at the *PAX6* locus detected by ChIP-qPCR during differentiation from D5 to D7 (Figures 3B, B'),
209 which becomes significant by D8 (Figures 2D, D'). In contrast with this apparently progressive decrease,
210 particularly in Jarid2 occupancy, H3K27me3 levels at the *PAX6* TSS and along the gene body remain
211 unchanged between D5 and D7 (Figure 3B') and drop dramatically only at D8 (Figure 2D''). These data
212 align decreasing PRC occupancy with increasing chromatin accessibility, while acute loss of H3K27me3
213 appears a later step that coincides with robust *PAX6* transcription.

214 Genome-wide comparison of accessibility patterns across TSSs and gene bodies in D3, D6 and D8
215 cells revealed that although global accessibility levels remained relatively constant over time, a clear peak
216 in accessibility appeared at D6 of this differentiation (Figure 3C). Detailed analysis comparing D3 and D8
217 identified 7877 regions with increased, and 11603 regions with decreased, accessibility (analysis
218 performed with diffReps with thresholds FDR ≤ 0.01 and log2FC ≥1). These regions of increased
219 accessibility correlate well with known active enhancer marks such as H3K4me1 and H3K27ac detected
220 in human embryonic spinal cord and brain (data from the ENCODE regulatory element database [67](see
221 Figure S1) and we termed these regions "neural sites". Analysis of these 7877 neural sites revealed that
222 they are associated with 4001 genes (Table S1) and that accessibility increased across the TSS and body
223 of these genes over time, with accessibility peaking at D6 (Figure 3C') – this included additional chromatin
224 opening across genes already accessible at D3 as well as new genes with increased accessibility by D8
225 (Figure 3D).

226 GO term analysis of the genes associated with regions of increased accessibility on days 5, 6 and
227 8 revealed terms related to neural development and showed a progression with more genes associated
228 with these terms over time (Figure 3E, Table S1). Focussing on the GO term Neurogenesis we selected 2
229 key neural progenitor genes in addition to *PAX6* and examined the ATAC-seq signal in detail around the
230 gene body. Chromatin accessibility around *RARB* and *GLI3* showed an increase similar to that associated
231 with *PAX6* as early as D5 (Figures 3F, F'). Overall, these findings indicate that coordinated regulation of
232 chromatin accessibility is a general mechanism that mediates the onset of neural gene transcription,
233 while analysis of PRC occupancy dynamics at the exemplar *PAX6* locus identifies this repression complex
234 as a target of such regulation.

235 **Figure 3 Progressive increase in human neural gene accessibility during *in vitro* differentiation** (A) ATAC-seq peak
236 tracks in NMP-L (D3), D5, D6 and NP (D8) cells for the genomic regions of *PAX6*, grey boxes are peaks within the
237 gene body, black boxes, peaks outside of the gene body and red box genomic region of a known *PAX6* enhancer;
238 (B-B'') ChIP-qPCR for Jarid2, Ring1B and H3K27me3on D5, D6 and D7 (n = 3 independent experiments, each
239 indicated by circles, triangles and diamonds, bar = average, error bars = SEM, no significant differences between
240 samples, t-test). (C-C') Metaprofiles comparing chromatin accessibility in NMP-L (D3) and NP (D8) cells along the
241 gene body genome-wide (C) and focussed on genes associated with increased accessibility in NPs (D8) (neural sites,
242 C') compared to NMP-L; (D) Venn diagram representing distribution of genomic regions more accessible in NPs (D8)
243 (neural sites) compared to NMP-L (D3) and their appearance over time (D5 and D6). Comparison of accessible
244 regions and associated genes on D5 and after D5, revealed ~19% of genes had additional accessible regions, while
245 the majority were found in newly accessible genes, similarly 40% of D6 genes with additional regions became more
246 accessible in NP (D8); (E) GO term analysis of genes associated with neural sites compared to NMP-L (D3) and genes
247 associated with more accessible chromatin regions on D5 and D6 out of the neural sites; (F-F') ATAC-seq peak tracks
248 in NMP-L (D3), D5, D6 and NP (D8) cells for the genomic regions of *RARB* (E) and *GLI3* (E') , grey boxes are peaks
249 within the gene body

250

251 **ERK1/2 dephosphorylation induces precocious polycomb protein dissociation and global increase in**
252 **chromatin accessibility at neural sites**

253 In chick and mouse embryos, FGFR inhibition elicits precocious *Pax6* transcription [16, 33] and FGFR and
254 ERK1/2 dephosphorylation (this study) decompact this gene locus. We therefore next tested whether
255 ERK1/2 signalling regulates polycomb protein occupancy and if such signalling globally directs chromatin
256 accessibility at our defined neural sites. To address this, we first tested whether inhibition of ERK1/2
257 signalling advances human neural differentiation *in vitro*; cells were cultured as in Figure 4A and exposed
258 to MEKi or DMSO cells during differentiation (Figure 4B) and *PAX6* transcript levels analysed by RT-qPCR.
259 This revealed precocious *PAX6* transcription beginning at D5 and peaking at D6 in the presence of MEKi
260 (Figure 4C). This correlated with changes in polycomb protein occupancy: MEKi exposure on D5 and D6
261 resulted in decreased Ring1B at the *PAX6* and control locus *HOXD11*, and Jarid2 levels also showed a
262 declining trend (Figures 4D, D' and supplementary Figure S2). Furthermore, reduced H3K27me3 levels at
263 the *PAX6* locus on D6 (Figure 4D'') correlated with maximum precocious *PAX6* transcription elicited by
264 inhibition of ERK1/2 signalling (Figure 4C).

265 To determine whether ERK1/2 activity acts globally to regulate chromatin accessibility around
266 neural differentiation genes we performed ATAC-seq on cells at D5 and D6 exposed to MEKi or DMSO
267 during differentiation. A comparison of all regions opening between NMP-L (D3) and D5 in control (2653
268 regions) and MEKi (3977 regions, associated with 417 newly-accessible genes, and 368 more accessible
269 genes) conditions, identified 2612 regions with additional chromatin accessibility following MEKi
270 treatment (Figure 4E, Table S2). Most of the MEKi induced regions of increased accessibility (2191, 55%)
271 belonged to the previously defined neural sites (Figure 3C'), while a further 1437 regions were unique to
272 MEKi treatment and not included in neural sites (Figure 4E). Analysis of D6 control and MEKi datasets
273 revealed a similar pattern, with 3512 additional regions of increased accessibility induced by MEKi
274 (associated with 593 newly accessible genes and 437 genes acquiring additional accessibility) (Figure 4E')
275 and while the majority coincide with neural sites, a further 1992 regions were detected outside of control
276 D6 and D8 data sets (Figure 4E' and see below).

277 To interpret the genome-wide chromatin accessibility changes induced by MEKi, we analysed the
278 GO biological processes associated with these gene cohorts. Strikingly, MEKi treatment on D5
279 corresponded to an increased representation of genes associated with key neural development terms
280 (Figure 4F). Moreover, at D6 of MEKi treatment, genes associated with later neural development, such
281 as synapse organisation, were specifically increased (Figure 4F'). We therefore analysed the GO terms for
282 genes associated with more accessible regions that were unique to the MEKi data sets on D5 and D6 and
283 found a strong bias towards later neuronal differentiation (Table S3). This suggests that MEKi treatment
284 leads to increased global accessibility at neural differentiation genes and the accelerated progression to

285 a more advanced differentiation cell state. Examining the ATAC-seq peaks at individual genes (*DCX,*
286 *GABRB2* and *PAX6*) supported the conclusions of the global ATAC-seq analyses, showing that peaks
287 increased over time and that this was advanced with MEKi treatment on D5 (arrowheads in Figures 4G-
288 G").

289 **Figure 4 ERK1/2 de-phosphorylation induces precocious *PAX6* expression, reduced polycomb protein occupancy**
290 **and H3K27me3 at this locus and increases accessibility of hundreds of neural differentiation genes** (A)
291 Differentiation protocol generating NMP-L (D3) cells and spinal cord NPs by D8 and additional treatment with
292 vehicle control DMSO or MEK inhibitor (PD184352, MEKi) every 24h during this differentiation; (B) Western blot
293 confirming that exposure to MEKi lead to reduced ERK1/2 phosphorylation after 24h in differentiation conditions
294 (D3-D4); (C) *PAX6* transcript levels in NMP-L (D3), in control conditions (WT and DMSO) or in MEKi treated cells on
295 D5 and D6 and NP(D8) determined by RTqPCR (n = 3 independent experiments indicated by circles, triangles and
296 diamonds, bar = average, error bars = SEM); (D-D'') ChIP-qPCR for Jarid2 and Ring1B and H3K27me3 on D6 (n = 3
297 independent experiments indicated with circles, triangles and diamonds, bar = average, error bars = SEM, * = $p \leq$
298 0.05, t-test); (E-E') Venn diagrams representing distribution of genomic regions that become more accessible on
299 D5 (E) and D6 (E') in control condition and MEKi treated cells compared to NMP-L (not restricted to regions
300 accessible in NPs (D8)) as well as more accessible regions on D8; (note comparing DMSO treated cells with untreated
301 cells revealed that these two conditions did not differ from each other on D5 or D6 (Figure S2); (F-F') GO term
302 analysis of genes associated with more accessible chromatin in D5 (F) and D6 (F') in control condition and MEKi
303 treated cells compared to NMP-L; (G-G'') ATAC-seq peak tracks in NMP-L, D5 DMSO and MEKi, D6 DMSO and MEKi
304 and NP (D8) cells for the genomic regions of *DCX* (G), *GABRB2* (G') and *PAX6* (G''), grey boxes outline peaks within
305 the gene body, black boxes peaks outside of the gene body and red box genomic region of a known *PAX6* enhancer,
306 example comparisons between peaks in MEKi and DMSO conditions indicated with black arrowhead pairs.

307

308 **De-phosphorylation does not alter ERK1/2 protein association with chromatin**

309 To investigate the mechanism by which ERK1/2 signalling maintains PRC occupancy at differentiation
310 genes we asked whether ERK1/2 acts directly to mediate recruitment of polycomb machinery, as
311 reported in mES cells [56]. ChIP-qPCR was first used to determine ERK1/2 occupancy across *PAX6* and
312 control genes during in vitro differentiation. In NMP-L cells, ERK1/2 was found at the *PAX6* TSS and gene
313 body and the *HOXD11* TSS and was also detected at the *GAPDH* TSS. Although ERK1/2 localisation at both
314 *PAX6* and *HOXD11* decreased in a manner consistent with increased accessibility of these loci during
315 differentiation, this also occurred at the locus of the constitutively transcribed gene *GAPDH* (Figure 5A).
316 We next analysed whether ERK1/2 occupancy is dependent on its phosphorylation status by treating cells
317 with MEKi during differentiation (as in Figures 4A). No statistical difference was found between MEKi
318 treated cells and control (untreated or DMSO treated) on either D5 or D6 (Figures 5B, B'). These data
319 reveal no consistent relationship between ERK1/2 chromatin association and gene transcription (ERK1/2
320 is found at the constitutively expressed *GAPDH* locus as well as *PAX6* and other loci) during
321 differentiation. Moreover, the pattern of ERK1/2 occupancy is unaltered upon its de-phosphorylation
322 indicating that change in ERK1/2 activity, but not its chromatin association, regulates PRC occupancy.

323 **Figure 5 ERK2-chromatin association does not correlate with PRC occupancy and is not regulated by ERK1/2 activity;**
324 **short ERK1/2 dephosphorylation in NMP-L cells attenuates PRC2 occupancy at the *PAX6* locus, without affecting**
325 **PRC1 occupancy, H3K27me3 levels or transcription.** (A) ChIP-qPCR detecting ERK1/2 occupancy at *PAX6* and control
326 loci during differentiation (NMP-L (D3), D5 and D6, black, dark grey and light grey respectively) (n = 3 independent
327 experiments, error bars = SEM, * = p ≤ 0.05, # = p= 0.055 t-test); (B and B') ChIP-qPCR investigating ERK1/2
328 occupancy at the *PAX6* locus on D5 and D6 of the differentiation protocol comparing untreated, DMSO and MEKi
329 exposed samples (n = 3 independent experiment, error bars = SEM, no significant differences between treatments,
330 t-test); (C) Differentiation protocol used to generate NMP-L (D3) cells and treatment regime with vehicle control
331 DMSO or MEKi for 3h; (D-D') representative Western blot of cell lysates probed with antibodies against total
332 (panERK1/2) and dual-phosphorylated-ERK1/2 (dpERK1/2) and LiCOR quantification data (n = 3 independent
333 experiments, error bar = SEM, * p= <0.05); (E-E'') ChIP-qPCRs investigating Jarid2 and Ring1B occupancy and
334 H3K27me3 levels at *PAX6* and control regions in NMP-L (D3) cells treated with MEKi or DMSO for 3h (n = 3 individual
335 experiments indicated with circles, triangles and diamonds, bar = average, no significant differences between
336 samples, t-test); (F-F'') transcription levels of *PAX6*, *HOXD11*, and *JARID2* assessed by RTqPCR in undifferentiated
337 cell (hESCs), untreated, vehicle control (DMSO) treated or MEKi treated NMP-L (D3) cells (n=3 individual
338 experiments, no significant differences between samples, t-test).

339

340 **Short duration ERK1/2 dephosphorylation in NMP-L cells suggests PRC2 loss initiates chromatin changes**

341 To uncover how ERK1/2 activity regulates PRC occupancy we next analysed the timing of Jarid2, Ring1B
342 and H3K27me3 loss from key loci following exposure of NMP-L (D3) cells to MEKi or DMSO (Figure 5C).
343 After only 3 hours, MEKi treatment (in the presence of FGF) reduced dpERK1/2 levels (Figures 5D, D').
344 Importantly, under these conditions ChIP-qPCR revealed no change in Ring1B nor H3K27me3 occupancy
345 (Figures 5E' and E''). However, there was a marked decrease in Jarid2 at *Pax6* and *HoxD11* loci (while
346 little H3K27me3, Ring1B and Jarid2 were detected at negative control loci in any condition) (Figure 5E).
347 This short exposure is therefore insufficient to disassemble the PRC1 (Ring1B) complex or remove the
348 H3K27me3 mark, but may initiate the departure of the PRC2 component Jarid2. Interestingly, no effects
349 on *PAX6* or *HOXD11* transcription, nor reduction in *JARID2* transcription were observed (Figures 3D-D'').
350 These data raise the possibility that ERK1/2 activity regulates PRCs by supporting Jarid2 occupancy and
351 suggest that Jarid2 dissociation is an initial step in the disassembly of this complex, distinct from later
352 mechanism(s) regulating transcriptional onset of target genes.

353

354 **Transient ERK1/2 dephosphorylation in NMP-L cells induces dissociation of both Jarid2 and Ring1b and**
355 **chromatin decompaction at the *PAX6* locus, but does alter H3K27Me3 nor elicit transcription**

356 To assess the consequences of loss of ERK1/2 activity at a later time point in NMP-L (D3) cells, these were
357 exposed to MEKi for 12 hours before conducting the same panel of ChIP-qPCR experiments (Figure 6A).
358 At the end of this period ERK1/2 phosphorylation levels had now returned to control levels (Figures 6B,
359 B', indicative of transient MEKi effectiveness), although other consequences of reduced ERK1/2 activity,
360 such as increased PKB phosphorylation were still apparent (Figure S3): this regime therefore delivers only

361 transient inhibition of ERK1/2 activity for at least 3h. However, after 12h reduced Jarid2 and also Ring1B
362 occupancy were now detected at *PAX6* and *HOXD11* loci in exposed cells (while control genomic regions
363 possessed only low level H3K27me3 and Ring1B and Jarid2, which did not change with MEKi
364 treatment)(Figure 6C-C'). Importantly, none of the gene loci analysed exhibited change in H3K27me3
365 levels (Figure 6C'') nor did the loss of both PRC1 and PRC2 proteins correlate with transcription of *PAX6*
366 or *HOXD11* nor with reduced *JARID2* transcripts in these conditions (Figures 6D-D'').

367 **Figure 6 Transient ERK1/2 dephosphorylation induces dissociation of Jarid2 and Ring1B and chromatin**
368 **decompaction in NMP-L cells at the *PAX6* locus, but does not reduce H3K27me3 nor elicit transcription** (A)
369 Differentiation protocol used to generate NMP-L (D3) cells and additional treatment with vehicle control DMSO or
370 MEKi for 12h; (B-B') representative Western blot of cell lysates probed with antibodies against total (panERK1/2)
371 and dual-phosphorylated-ERK1/2 (dpERK1/2) and LiCOR quantification data (n = 3 independent experiments, error
372 bar = SEM); (C-C'') ChIP-qPCRs investigating the histone modification H3K27me3 and polycomb repressive complex
373 occupancy in NMP-L (D3) cells treated with MEKi or DMSO for 12h (n = 3 individual experiments indicated with
374 circles, triangles and diamonds, bar = average, * = p≤ 0.05, t-test); (D-D'') Transcription levels of *PAX6, HOXD11*, and
375 *JARID2* assessed by RT-qPCR in undifferentiated cell (hESCs), NMP-L cells untreated, vehicle control (DMSO) treated
376 or MEKi treated (n=3 individual experiments, no significant differences between samples, t-test); (E-E') FISH to
377 assess chromatin compaction around the *PAX6* locus in NMP-Ls untreated and treated with DMSO or MEKi for 12h.
378 2 probes flanking the target locus (inter-probe distance ca 51 kb) were hybridised and visualised by differential
379 labelling nuclei (outlined with white dashed line) visualised with DAPI (blue). Inter-probe distance measurements in
380 >50 nuclei in the three conditions in three individual experiments (n = > 150 nuclei/cell type, Mann Whitney -
381 test/RankSum-test, *** p ≤ 0.001), this decompaction correlated with a 2.5 fold decrease in number of base pairs
382 per nm compared to both controls (untreated NMP-L (D3): 205 bp/nm, DMSO NMP-L (D3): 218 bp/nm and MEKi
383 NMPL (D3): 87 bp/nm).

384 These data indicate that a transient reduction in ERK1/2 signalling is sufficient to trigger loss of
385 both PRC2 and PRC1 proteins. To determine the significance of such loss in this context, we further
386 assessed whether 12h MEKi exposure also altered chromatin accessibility around the *PAX6* locus using
387 FISH. Significant decompaction of this region was found in MEKi treated cells compared with both DMSO
388 and untreated controls (Figures 6E, E'). These findings correlate PRC loss with a distinct increase in
389 chromatin accessibility across this key neural progenitor gene and in showing that this step is not
390 reinstated on resumption of ERK1/2 activity, suggest that this is a directional molecular mechanism.
391 Moreover, these data demonstrate that removal of H3K27me3 is not required for such chromatin re-
392 organisation and indicate that regulation of this histone modification is molecularly distinct from the
393 initial effects of ERK1/2 dephosphorylation, indeed this correlated well with later transcriptional onset
394 (Figures 6C - C'' compare Figures 2 D-D''). These distinct steps are summarised in Figure 7.

395 **Figure 7 Summary model** Decline in Fibroblast Growth Factor (FGF) and downstream effector kinase ERK1/2
396 signalling as caudal epiblast cells commence differentiation leads to loss of polycomb repressive complexes (PRC2
397 and PRC1) from exemplar neural differentiation gene *PAX6* and chromatin decompaction across this gene locus:
398 such reduction in ERK1/2 activity induces genome-wide increase in chromatin accessibility across neural genes.
399 Histone modifications H3K4me3 and H3K27me3 are both detected (bivalent configuration) in the presence of FGF
400 and following dissociation of PRCs, and the PRC-mediated gene silencing mark H3K27me3 is lost only later
401 coincident with transcriptional onset: this indicates that this is a distinct regulatory step, which may depend on
402 retinoic acid (RA) signalling which is known to be required for *PAX6* transcription. As transient loss of ERK1/2 activity
403 is sufficient to remove PRC2 and PRC1 and these complexes are not re-imposed on resumption of ERK1/2 signalling,
404 regulation of ERK1/2 activity and so PRC occupancy constitutes a directional molecular mechanism that
405 synchronises neural gene accessibility and promotes engagement of the neural differentiation programme.

406

407 **Discussion**

408 In this study, we uncover the molecular mechanism by which the neural inducing signal FGF regulates
409 higher order chromatin organisation to orchestrate engagement of the neural differentiation
410 programme. We demonstrate that loss of the activity of FGF-effector kinase ERK1/2 leads to rapid
411 chromatin decompaction at the neural gene *PAX6* in both the caudal lateral epiblast of mouse embryos
412 and in analogous hESC-derived NMP-L cells. Using ATAC-seq we show that this reflects a global action
413 involving increased chromatin accessibility across hundreds of neural genes. Focussing on *PAX6* as an
414 exemplar gene, we find that ERK1/2 dephosphorylation specifically results in removal of polycomb
415 proteins, while ERK1/2 association with chromatin at this locus is unaltered. This demonstrates that
416 ERK1/2 activity and not occupancy is critical for this mechanism. We further show that while *PAX6* is a
417 bivalent gene that is poised to be expressed in NMP-L cells, PRC protein loss following ERK1/2 inhibition
418 is distinct from later actions that mediate removal of the gene silencing mark H3K27me3 and
419 transcriptional onset. Importantly, transient ERK1/2 inhibition was sufficient to trigger PRC loss and
420 increased chromatin accessibility, indeed polycomb protein occupancy was not reinstated on resumption
421 of ERK1/2 signalling, indicating that this is a directional molecular mechanism that advances
422 differentiation. These findings suggest a model in which FGF/ERK1/2 signalling promotes or maintains
423 PRCs at neural gene loci while its subsequent decline during development initiates the neural programme
424 by synchronising removal of this repressive complex and so the increased accessibility of neural genes
425 (Figure 7).

426

427 The ability of ERK1/2 inhibition to elicit chromatin decompaction at the *PAX6* locus in both the
428 mouse embryo and human ESC derived NMP-L cells indicates that the molecular mechanism by which
429 ERK1/2 regulates chromatin accessibility is conserved across species. Establishing *PAX6* as a polycomb
430 target in both contexts further identified this repressive complex as the likely mediator of chromatin
431 compaction. PRC1-generated compaction has been demonstrated and elucidated in mESCs [68-71] and
432 *Pax6* has recently been identified as a PRC target in this context too [72]. The rapid decompaction of
433 chromatin (within just one hour) following ERK1/2 inhibition in the mouse embryo shown here further
434 suggested that ERK1/2 activity may directly maintain PRC occupancy. Exposure of differentiating human
435 NMP-L cells to MEKi lead to loss of PRC1 component Ring1B, while PRC2 protein Jarid2 was not
436 significantly changed. This raises the possibility that PRC1 dissociates first and is the primary target of
437 ERK1/2 activity and PRC2 is lost secondarily. However, Jarid2 occupancy does show a marked downward
438 trend following ERK1/2 inhibition and the lack of significant difference may reflect low amounts of Jarid2
439 protein at chromatin or differences in antibody effectiveness. In support of the initial loss of PRC2, we
440 found that inhibition of ERK1/2 in NMP-L cells (which were maintained in FGF and Wnt agonist) for 3h

441 elicited a declining trend in Jarid2 occupancy at the *PAX6* locus and that only after 12h were both Jarid2
442 and Ring1b significantly reduced. Importantly, in these experiments in NMP-L cells H3K27me3 levels
443 remained unchanged and no *PAX6* transcription was detected. These findings are consistent with
444 observations in Ring1B deficient mouse ES cells, where chromatin decompaction occurred at the *HoxB*
445 and *D* loci that remained decorated with H3K27me3 at the gene promoters [68]. Although there are
446 examples of transcription from loci carrying H3K27me3 [36, 73], our findings here indicate that
447 H3K27me3 removal is closely associated with the transcriptional de-repression of *PAX6.* These findings
448 emphasise the value of the temporal resolution afforded by this *in vitro* differentiation assay to decouple
449 the molecular mechanisms regulating chromatin accessibility from those directing transcription initiation.

450 Using ATAC-seq we identified genes with increasing accessibility during neural differentiation and
451 surveyed the global consequences of MEK inhibition in NMP-L cells in differentiation conditions;
452 uncovering genes with increased accessibility on day 5, prior to precocious transcription of *PAX6* (on day
453 6). This identified hundreds of genes with GO terms associated with neural development. These included
454 *PAX6*, but also other neural progenitor genes, (e.g. *SOX1, Gli3, Gli2, RARB, NKX6.1, DBX1, NEUROG2,*
455 which commence expression in the embryonic body axis, like *Pax6*, after FGF/ERK1/2 signalling decline
456 [16, 18, 31]). These data indicate that loss of ERK1/2 signalling accelerates differentiation progression by
457 increasing chromatin accessibility at many early neural genes. The extent to which such genes are direct
458 PRC targets or are regulated by other de-repressed neural genes remains to be determined, however,
459 their increased accessibility on D5, prior to *PAX6* transcription, supports the possibility that they are also
460 PRC targets.

461 There are a number of ways in which ERK1/2 activity may influence PRC occupancy at neural
462 genes. Work in mES cells has shown that ERK1/2 occupies overlapping targets with polycomb proteins
463 and in particular Jarid2 and that abrogating ERK1/2 signalling reduces Jarid2 and H3K27me3 levels raising
464 the possibility that ERK1/2 protein is directly involved in PRC recruitment and/or maintenance [56].
465 Although we detected ERK1/2 at the *PAX6* locus and observed a decline in occupancy during
466 differentiation, we also found this protein at the house-keeping gene *GAPDH*, indicating that in this
467 context its association with DNA is not PRC target gene specific. Furthermore, inhibition of ERK1/2 activity
468 did not alter its association with chromatin at the *PAX6* locus. This indicates that decrease in ERK1/2
469 activity and not ERK1/2 occupancy correlates with reduced PRC present at the *PAX6* locus in
470 differentiating NMP-L cells. This differs from observations made in mES cells where MEKi exposure leads
471 to an overall reduction in ERK2 occupancy at developmental genes [56]. This might reflect operation of
472 distinct regulatory mechanisms in these different cellular contexts, indeed ERK inhibition promotes self-
473 renewal in the mouse ES cell state, while loss of FGF and so ERK promotes differentiation progression of
474 human ESC and of NMP-L cells. Moreover, the observation that NMP-L cells exposed to MEKi lose PRC

occupancy and decompact at the *PAX6* locus, despite resumption of ERK1/2 signalling (in the continued presence of exogenous FGF), indicated that the effects of ERK1/2 inhibition are not easily reversed in NMP-L cells. This contrasts with findings in mES cells, where rescue of ERK1/2 mutant ESCs with ERK2 restored PRC mark H3K27me3 [56]. Loss of ERK1/2 signalling for a short and transient period in NMP-L cells therefore appears sufficient for sustained PRC dissociation and increased chromatin accessibility in this cell context and this provides directionality, triggering consequences which promote differentiation progression. In this sense, decline in ERK1/2 signalling here appears to be an initial step in the process of neural commitment.

In addition to potential regulation of PRC protein phosphorylation by the kinase activity of ERK1/2, a further possibility is that ERK1/2 signalling decline alters BAF (or SWI/SNF) complex composition, leading to its recruitment and so eviction of PRC proteins from gene loci, as reported in mouse fibroblasts and ESCs [74]. This is an attractive possibility as it might also provide specificity for PRC removal at neural genes, encoded in BAF complex composition [75]. This complex alters as neural progenitor cells become post-mitotic and embark on neuronal differentiation [75, 76], while here we would expect loss of ERK1/2 activity to lead to initial formation of the BAF complex characteristic of neural progenitors. In support of such a step, the transcription of key BAF complex component the ATP-dependent helicase *SMARCA2* (Brahma homolog) is sharply downregulated as FGF/ERK1/2 signalling declines in the elongating embryonic body axis [77].

The extent to which FGF/ERK1/2 signalling directs progression of differentiation by regulating PRC occupancy in contexts other than caudal epiblast/NMP-L cells requires further investigation. In mouse ESCs maintained in serum and LIF, PRC and H3K27me3 are detected at differentiation gene loci and this constitutes primed pluripotency, characterised by heterogenous cell states in a dynamic flux between pluripotency and differentiation [55, 78]. This contrasts with the ground-state or naïve pluripotent cell state achieved by treatment with both ERK1/2 and GSK3β inhibitors (2i) [25, 79], in which differentiation genes lack both PRC and H3K27me3 [55]. Importantly, differentiation of such 2i ES cells involves progression through the primed pluripotent cell state, suggesting that this involves recruitment of PRC and establishment of bivalent loci. Progression towards differentiation involves FGF/ERK1/2 signalling [28, 80] but only a transient period is required to initiate this process [27]. This last step is also consistent with the differentiation of mEpiSCs and hESCs (for which FGF is a self-renewal factor) when FGF signalling is blocked [30, 32]. The more homogenous neural differentiation achieved by expsoure of differentiaing mEpiSCs to Fgf8 [81], might also reflect more uniform recruitment of PRC. These observations together with the requirement for PRC1 and 2 for mESC differentiation [61], indicate a good correlation between exposure to a suffcient period of FGF/ERK1/2 signalling, PRC presence at

508 differentiation genes and subsequent differentiation from the ES cell state, following ERK1/2 signalling
509 decline.

510 Importantly, PRC occupancy is also associated with multiple steps that ready genes for
511 transcription. In mouse ES cells, the presence of PRCs coincides with that of poised (phosphorylated at
512 Ser5) RNA polymerase 2 (RNAPII), as well as with the presence of both active and repressive histone
513 marks, as observed here for *PAX6* in NMP-L cells [34, 40, 82-85]. A role for the PRC2 associated protein
514 Jarid2 in recruitment of poised RNAPII has also been proposed in mES cells [47]. The striking association
515 of poised RNAPII with polycomb silenced genes in neurons, further implicates PRC occupancy with
516 potential promoter plasticity in differentiated cells [40]. Moreover, PRC2 has been shown to mediate
517 engagement of poised enhancers with their target genes during anterior neural induction from mESCs
518 [86]. In addition, an in vitro interaction study has identified a role for ERK1/2-mediated phosphorylation
519 of Ser5 on RNAPII at PRC2 occupied loci in mES cells [56]. These findings, together with our observation
520 that ERK1/2 activity is required for PRC occupancy at *PAX6* in NMP-L cells and that its inhibition triggers
521 precocious *PAX6* transcription in differentiation conditions, suggest that promotion of PRC at neural
522 genes by ERK1/2 signalling functions as a rite of passage for subsequent differentiation. It will be
523 important to investigate whether such a mechanism operates not only to maintain, but also to poise for
524 subsequent synchronous differentiation, other FGF-expressing progenitor cell populations undergoing
525 expansion in the developing embryo, including in limb, lung and tooth buds [87-90] as well as distinct
526 regions of the nervous system [91]. Intriguingly, recent progress in understanding cell fate commitment
527 during epidermal homeostasis has identified a requirement for the ERK1/2/MAPK phosphatase DUSP6
528 for differentiation in this adult tissue context [92], underscoring the idea that transient ERK1/2 /
529 polycomb mediated chromatin regulation and associated gene poising constitute core and conserved
530 molecular machinery that is a prelude to cellular differentiation.

Materials and Methods

Embryo dissection and hanging drop culture

CD1 mouse embryos collected at embryonic stage E8.5 were dissected in warm medium (DMEM-F12 with 10% FBS, Gibco®) and one half the litter exposed MEK inhibitor (PD184532, MEKi, 3 µM final concentration, Enzo Life Sciences) and the other half exposed to vehicle control DMSO (equal volume, 1:4000). Each embryo was placed in a drop of medium in the lid of a 35 mm plate, which was flipped over onto its base, resulting in a hanging drop [93]. Embryos were cultured in a humid chamber at 37°C and 5% CO_2 for 1 h before fixation and processing for fluorescence in situ hybridisation (FISH) or chromatin immunoprecipitation (ChIP). All animal husbandry and procedures were approved by the UK Government Home Office and were in accordance with European Community Guidelines (directive 86/609/EEC) under project licence number 6004454.

Cell culture of human ESCs

Human ES cells(H9, WiCell) were cultured in ES medium and provided for experiments by the Human Pluripotent Stem Cell Facility of the University of Dundee. For differentiation, cells were plated on Geltrex® (Invitrogen) coated dishes at 10^3 cells/ cm^2. To generate neuromesodermal progenitor-like cells (NMP-L), ES media was removed and cells were cultured with neurobasal medium (Gibco®) supplemented with N2, B27, GlutaMAX™ (final concentration for each 1x, Gibco®), 20 ng/ml bFgf (Peprotech) and 3 µM CHIR99021 (Tocris Bioscience) for 3 days (after [13]). To generate neural progenitor cells (NPs) from these NMP-Ls bFgf and CHIR99021 were removed from the medium and the cells grown for further 5 days. From day 2 to day 4 the medium was additionally supplemented with BMP and TGFβ inhibitors (Noggin, Peprotech and SB431542, Tocris Bioscience). Treatment with MEK inhibitor (PD184352, MEKi, 3 µM) or DMSO (equal volume) was administered with the culture medium in a dilution of 1:4000 for transcript level analysis and ChIP-qPCR experiments and 1:20,000 in ATAC-seq experiments.

Fluorescence in situ hybridisation (FISH)

The mouse Pax6 fosmid pair (WIBR-1 Mouse Fosmid Library, Whitehead Institute/MIT Center for Genomic Research) and the human Pax6 BAC clone pair (WIBR-2 Human Library, see Table S3) were prepared using a standard Mini-prep protocol. Using Nick transcription the fosmids and BAC clones were labelled with Digoxigenin-11-dUTP and Biotin-16-dUTP. Unincorporated nucleotides were removed with Quick Spin G50 Sephadex columns (Roche) and labelled probes quantified by dot blotting.

Embryos were exposed for short term to MEKi or vehicle control DMSO by 1h hanging drop culture, then fixed (4% PFA, overnight), washed and dehydrated through a methanol series before being cleared in xylene and embedded in paraffin for sectioning (7 µm).

563 The FISH protocol on mouse tissue was adapted from (Newsome et al., 2003). Coverslips with sections
564 containing neural tube or caudal lateral epiblast tissue were heated to 65°C for 30 min, then xylene
565 washed (4 x 10 min each) and re-hydrated through an ethanol series to dH_20. The coverslips were
566 microwaved for 20 min in 0.1 M citrate buffer, pH 6.0, then left to cool and washed in dH_20. For probe
567 hybridisation, 150 ng each of the labelled probes together with 15 µg mouse Cot1 DNA and
568 5 µg sonicated salmon sperm DNA were denatured and incubated overnight at 37°C. After a series of
569 washes the probes were detected using FITC conjugated anti-Digoxigenin antibody (1:20, Roche)
570 amplified with anti-sheep Alexa Fluor 488 (1:100, Molecular Probes) and biotinylated anti-Avidin (1:100)
571 together with Alexa streptavidin 594 (1:500, Molecular Probes); nuclei were counterstained with DAPI,
572 coverslips were mounted with Slowfade Gold (Molecular Probes) and imaged on a Deltavision (Applied
573 Precision).

574 For FISH on human ESC derived cells, cells were directly grown and differentiated on glass coverslips
575 coated with Geltrex® and cells were untreated, exposed to DMSO or MEKi in DMSO as above. After a
576 short fixation (10 min, 4% formaldehyde, RT) the coverslips were washed in 0.05% Triton X-100/PBS (3 x
577 5 min, RT). For permeabilisation the coverslips were incubated in 0.5% Triton X-100/PBS for 10 min, then
578 transferred to 20% glycerol/PBS for 1h at 4°C and then repeatedly dipped in liquid nitrogen until
579 completely frozen, let to thaw and soaked in 20% glycerol/PBS again (6 repeats). After the last snap
580 freezing the coverslips were washed in 0.05% Triton X-100/PBS (3 x 5 min, RT), rinsed and incubated in
581 0.1 N HCl (10 min, RT) and washed in 0.05% Triton x-100/PBS (3 x 5 min, RT) again. To equilibrate,
582 coverslips were washed in 2xSSC before pre-hybridisation (50% Formamide in 2xSSC) for 30 min at RT.
583 For probe hybridisation, the same probe mix as for the FISH on mouse material was used (except probes
584 specific for the human *Pax6* locus). The probes were denature on a heat block at 75°C for 3 min before
585 hybridisation (overnight, 37°C, humid chamber). The coverslips were then washed and probes were
586 detected using the same antibody reactions as for the FISH on mouse samples; nuclei were
587 counterstained with DAPI, coverslips were mounted with Slowfade Gold and imaged using a widefield
588 Deltavision Microscope.

589 Using OMERO insight regions of interest (ROIs) were selected over at least 3 z-sections. The 3D inter-
590 probe distances in ROIs were measured using a custom script called OMERO mtools) [94], by segmenting
591 the objects from the background and calculating the distance between the centroids as d in µm. For ease
592 of comparison the ratio of number of base pairs per nm was calculated using the inter-probe distance
593 known in bp and measured in nm.

594 Chromatin immunoprecipitation (ChIP)

595 For each IP and control IP 25 µL of dynabeads coated with protein A (Invitrogen) were used. Beads were
596 washed 3 times in blocking buffer (0.1% BSA in PBS) and resuspended in blocking buffer containing the

597 antibody for immunoprecipitation or an equal amount of unspecific IgG (see Table S4) and incubated for
598 2 to 3h at 4°C. Beads were then washed twice in blocking buffer, resuspended in blocking buffer and
599 stored at 4°C until immunoprecipitation.

600 For ChIP on human ES cells, the cells were grown and differentiated in 10 cm culture dishes at 37°C and
601 5% CO_2. Cells were fixed with formaldehyde (Sigma-Aldrich®, 1%, 10 min, RT) and quenched with glycine
602 (0.125 M, 5 min, RT). Cells were then washed 3 times with PBS and harvested by scraping into protein
603 low bind Eppendorf® tubes and centrifuged (4000 x g, 10 min, 4°C). The pellets were snap frozen on dry
604 ice and stored at -80°C. For the chromatin preparation, the cell pellet was resuspended in lysis buffer
605 (50 mM Tris-HCl, pH 8.1; 10 mM EDTA, pH 8; 1% SDS and protease inhibitor), vortexted and incubated
606 (10 min on ice). Chromatin fragments of approximately 500 to 1000 bp were generated by sonication
607 with a probe sonicator (Vibra-Cell, Sonics®, 8 cycles, 30s on, 30s off, 30% amplitude). Sonicated lysate
608 was diluted (1:5) in dilution buffer (20 mM Tris-HCl, pH 8.1; 150 mM NaCl; 2 mM EDTA pH 8.1% Triton
609 X-100 and protease inhibitor) and centrifuged (20 min, full speed, 4°C). The supernatant was transferred
610 into a fresh tube. DNA concentration was determined with NanoDrop 2000 Spectrophotometer.

611 For ChIP of chromatin associated proteins 100 µg of chromatin and ChIP of histone modifications 25 µg
612 of chromatin was diluted to a final volume in 1 mL, added to the already prepared bead-antibody
613 complexes and incubated (overnight, 4°C , rotating). An input for each ChIP (10% of ChIPed amount) was
614 kept at -20°C. The next day, beads were washed 5 times in wash buffer (100 mM Tris, pH8.8; 0.5 M LiCl;
615 1% NP-40, 1% NaDoc and protease inhibitor) and then rinsed and washed in 1x TE (10 mM Tris and 1 mM
616 EDTA, pH 8). To elute the beads were resupended in elution buffer (50 mM Tris-HCl, pH 8; 10 mM EDTA,
617 pH 8; 1% SDS) and incubated (15 min, 65 °C, 1400 rpm). The eluate was spun down quickly and the
618 supernatant was transferred into a fresh tube. Formaldehyde crosslinking was reversed by incubation at
619 65°C and 700 rpm for 6 h. The input sample was diluted with elution buffer (1:1) and crosslinking
620 reversed. All samples were then diluted with TE (1:1) and RNA and proteins were digested (RNAse, Sigma-
621 Aldrich®, 30 min, 37°C and proteinase K, Sigma-Aldrich®, 90 min 45°C). DNA was recovered by
622 Phenol/Chloroform extraction (Phenol:Chloroform:Isoamylalcohol,25:24:1, pH 8, Sigma-Aldrich®) and
623 washed with Chloroform:Isoamylalcohol (24:1, Amresco®) and then precipitated in 96% ice cold ethanol,
624 with 3 M Na-Acetate and linear polyacrylamide (5 mg/mL, Ambion®) overnight at -80°C. Precipitated DNA
625 was washed with 70% ice cold ethanol and pellet was air dried before resuspension in nuclease free
626 water.

627 A similar protocol was used to ChIP material from caudal mouse explants. 30 caudal explants were pooled
628 and resuspended in lysis buffer, vortexed and dissociated by pipetting before incubating on ice for 10
629 min and sonication. The lysate was diluted in dilution buffer, centrifuged (20 min, maximum speed, 4°C),
630 the supernatant was transferred into a new tube (and the DNA concentration determined by NanoDrop

631 2000 Spectrophotometer .25 µg of chromatin were used to immunoprecipitate with 3 µg of the rabbit
632 anti H3K27me3 antibody (Millipore) previously bound to dynabeads overnight at 4°C. After that the same
633 procedure of washing, eluting, uncrosslinking and precipitation of DNA was used.

634 For quantification of specifically immunoprecipitated DNA, quantitative real time PCR was performed
635 (PerfeCTa® SYBR® Green SuperMix for iQ™, Quanta Biosciences or Brilliant III Ultra Fast QPCR Master Mix,
636 Agilent Technologies). Each sample was analysed in 3 biological replicates and each biological replicate
637 was analysed in technical triplicates using primer pairs in Table S5.

638 Transcription level analysis by reverse transcription quantitative PCR (RTqPCR)

639 For RNA extraction human ES cells were grown and differentiated in 24 well plates. Cells were washed
640 with PBS before being collected in 350 µL of lysis buffer from the Qiagen RNeasy Mini Kit and RNA was
641 prepared according to manufacturer's protocol. An on-column DNA digest with RQ1 RNase-
642 Free DNase (Promega) was performed (RT, 15 min). cDNA was generated from 500 µg purified RNA with
643 the ImProm-II™ Reverse Transcription System (Promega) primed by random primers. The Aria Mx real
644 time PCR system with the Brilliant III Ultra-Fast QPCR Master Mix (Agilent Technologies) was used to
645 quantify the transcript levels. Each sample was analysed in biological triplicate and each biological
646 replicate was run in technical triplicates (for primers see Table S6). The relative transcription level of a
647 gene was normalised to that of *GAPDH* using the Pfaffl method [95] and *GAPDH* levels were checked by
648 normalisation to HPRT1.

649 Western Blotting

650 A minimum of 4 stage E8.5 mouse embryos or human ES cells grown in a 6 well plate were lysed in lysis
651 buffer (LB Nuc+ all) ,kept on ice for 30 min while vortexing every 5 min and centrifugation (maximum
652 speed, 4°C, 20 min). The supernatant was transferred into a new tube and protein concentration
653 determined by Bradford assay. 50 µg of protein were separated on a 4-12% precast Gel (Invitrogen) in 1x
654 MES buffer (Invitrogen) next to a size marker before they were blotted onto a PVDF membrane in transfer
655 buffer (25 mM Tris, 190 mM glycine, 20% methanol). To minimise variances, every sample was loaded
656 twice on the same gel and blotted onto a membrane at the same time. After blotting the membrane
657 halved and one half was processed with a pan antibody and an antibody for the loading control α-Tubulin
658 and the other half with a phosphorylation specific antibody and the loading control antibody. Membranes
659 were first blocked in 3% BSA in TBST for at least 2h at RT, before incubation with primary antibody (see
660 Table S7) overnight. After washing in TBST (3 x 10 min, RT) the membrane was incubated with secondary
661 antibodies (see TableS7, 90 min, RT). Following TBST washes signals were visualised by scanning on LI-COR
662 Odyssey® system. Band intensity measurements were performed for quantification. The loading controls
663 were used to normalise for minor differences in loading before the phosphorylated ERK1/2 or PKB levels
664 were compared to the pan ERK1/2 and PKB levels of the same samples.

665 ATAC-seq

666 Experimental procedure

667 ATAC seq was performed on NMP-L cells, D5 and D6 cells in untreated, DMSO treated or MEKi treated
668 condition and NP (D8) cells with the following modifications to the method described by Buenrostro and
669 colleagues [65, 96]. Cells were treated with TrypLE™ Select (Thermo Fisher) to obtain a single cell
670 suspension. Cells were then resuspended and counted in ice cold PBS and 50 000 cells per sample were
671 used for the ATAC protocol (biological replicates were collected from independent experiments). Cells
672 were pelleted and resuspended in lysis buffer (10mM Tris-HCl pH 7.4, 10mM NaCl, 3mM $MgCl_2$, 0.1% NP-
673 40) and centrifuged (10 min, 4°C). Nuclei extracts were resuspended in transposition buffer for 4 h at
674 37°C. The reaction was purified using the Qiagen MinElute PCR Purification kit according to
675 manufacturer's instructions. To generate single-indexed libraries the transposed DNA was PCR amplified
676 with Nextera primers [65]. Library quality was assessed using Agilent TapeStation D5000 High Sensitivity
677 Screen Tapes or a High Sensitivity DNA analysis kit for the Bioanalyzer.

678 Library-level analysis

679 Sequencing was performed by multiplexing 4 samples per lane on the Illumina HiSeq 2500 platform
680 (Francis Crick Institute). This typically generated ~86 million 51bp or 101bp paired-end reads per library.
681 Raw reads from each sample were adapter-trimmed using cutadapt (version 1.9.1) [97] with parameters
682 "-a CTGTCTCTTATA -A CTGTCTCTTATA --minimum-length=25 –quality-cutoff=20". If required, the
683 additional parameters "-u <trim_length>" and "-U <trim_length>" were provided to cutadapt in order to
684 trim all reads to 51bp. BWA (version 0.6.2) [98, 99] with default parameters was used to perform genome-
685 wide mapping of the adapter-trimmed reads to the human hg19 genome assembly downloaded from the
686 UCSC [100]. Read group addition, duplicate marking and insert size assessment was performed using the
687 picard tools AddOrReplaceReadGroups, MarkDuplicates and CollectMultipleMetrics, respectively
688 (version 2.1.1) (http://broadinstitute.github.io/picard). Reads mapped to mitochondrial DNA were
689 removed using the pairToBed command from BEDTools (version 2.26.0-foss-2016b) [101]. Additional
690 filtering was performed to only include uniquely mapped, properly-paired reads with insert size <= 2kb,
691 and mismatches <= 1 in both reads. Samtools (version 1.3.1) [98] was used for bam file sorting and
692 indexing. The filtered alignments from each library were merged at both the replicate and sample level
693 using the picard MergeSamFiles command. Duplicate marking and removal was reperformed on the
694 merged alignments. BedGraph coverage tracks representing the accessibility signal per million mapped
695 reads were generated using BEDTools genomeCoverageBed with the parameters "-bg -pc -scale
696 <SCALE_FACTOR>". BedGraph files were converted to bigWig using the wigToBigWig binary available
697 from the UCSC with the "-clip" parameter [102].

698 Sample-level analysis

699 To define peaks, regions of chromatin accessibility were identified genome-wide using MACS2 callpeak
700 (version 2.1.1.20160309) [103] with the parameters "--gsize=hs --keep-dup all –f BAMPE --nomodel--
701 broad". A consensus set of intervals were obtained by merging the regions identified across all samples.

702 Replicate-level analysis

703 Fragment-level BED files were derived from those created using the BEDTools bamToBed command with
704 the option "-bedpe". Differential chromatin accessibility sites between conditions were obtained using
705 diffReps (version 1.55.4) [104] with the parameter "—frag 0". The annotatePeaks.pl program from
706 HOMER (version 4.8) [105] was used to annotate the differential sites relative to the nearest gene
707 promoter with respect to hg19 RefSeq features downloaded from the UCSC on 7th June 2017. Differential
708 sites for each comparison were defined as those that intersected with the consensus set of accessibility
709 sites, had an FDR <= 0.01 and fold-change >= 2, and an annotated gene symbol regardless of distance to
710 TSS. Differential sites that were not allocated a gene symbol were not carried forward for further analysis.
711 Genes associated with differential chromatin accessible regions as identified with ATAC-seq were used
712 as input for gene ontology analysis using https://go.princeton.edu/.- ATAC-seq metaprofiles were
713 generated using deepTools (version 2.5.3) [106] with the "computeMatrix scale-regions" and
714 "plotHeatmap" commands, respectively. The genome annotation was generated by taking the minimum
715 and maximum genomic coordinates amongst all the isoforms for a given gene. Raw ATAC-seq data and
716 normalised replicate-level bigWig files have been deposited in the NCBI Gene Expression Omnibus (GEO)
717 under accession code GSE121126) (access token provided to the journal editor).

718

719

Acknowledgements

We thank Lindsay Davidson (University of Dundee, Human Pluripotent Cell Facility) for provision of quality controlled hES cells. We are grateful to Laure Verrier for sharing human NMP-L cell generation and neural differentiation protocols and her expertise in chromatin IP techniques as well as for critical discussions. We are also grateful to Peter Rugg-Gunn, Stephen Keyse, Josh Brickman, Greg Findlay and Tom Owen-Hughes as well as members of the Storey group for critical comments on versions of this manuscript. The authors thank the ENCODE Consortium and the ENCODE production labs of Bradley Bernstein, John Stamatoyannopoulos and Joseph Costello for data sets queried here. CS was supported by a BBSRC studentship (1252451) and KGS is a Wellcome Trust Investigator (WT102817AIA). JB, VM and HP are supported by the Francis Crick Institute which receives its core funding from Cancer Research UK (FC001051), the UK Medical Research Council (FC001051), and the Wellcome Trust (FC001051). We are grateful to the Francis Crick institutes' Advanced Sequencing Facility.

Author contributions

All experiments were carried out by CS who worked together with KGS to design experiments, analyse data and write the paper. JB VM and HP performed ATAC-seq experimental design and analysis and revised the paper.

Declaration of interest

The authors declare no conflicts of interest.

741 References

742 1. Delaune E, Lemaire P, Kodjabachian L. Neural induction in Xenopus requires early FGF signalling in addition
743 to BMP inhibition. Development. 2005;132(2):299-310. PubMed PMID: 15590738.

744 2. Lamb TM, Harland RM. Fibroblast growth factor is a direct neural inducer, which combined with noggin
745 generates anterior-posterior neural pattern. Development. 1995;121(11):3627-36.

746 3. Storey KG, Goriely A, Sargent CM, Brown JM, Burns HD, Abud HM, et al. Early posterior neural tissue is
747 induced by FGF in the chick embryo. Development. 1998;125(3):473-84.

748 4. Streit A, Berliner AJ, Papanayotou C, Sirulnik A, Stern CD. Initiation of neural induction by FGF signalling
749 before gastrulation. Nature. 2000;406(6791):74-8.

750 5. Londin ER, Niemiec J, Sirotkin HI. Chordin, FGF signaling, and mesodermal factors cooperate in zebrafish
751 neural induction. Developmental biology. 2005;279(1):1-19. Epub 2005/02/15. doi: 10.1016/j.ydbio.2004.11.016.
752 PubMed PMID: 15708554.

753 6. Rentzsch F, Bakkers J, Kramer C, Hammerschmidt M. Fgf signaling induces posterior neuroectoderm
754 independently of Bmp signaling inhibition. Developmental dynamics : an official publication of the American
755 Association of Anatomists. 2004;231(4):750-7. Epub 2004/11/09. doi: 10.1002/dvdy.20244. PubMed PMID:
756 15532058.

757 7. Sheng G, dos Reis M, Stern CD. Churchill, a zinc finger transcriptional activator, regulates the transition
758 between gastrulation and neurulation. Cell. 2003;115(5):603-13. PubMed PMID: 14651851.

759 8. Stern CD. Neural induction: 10 years on since the 'default model'. Current opinion in cell biology.
760 2006;18(6):692-7. Epub 2006/10/19. doi: 10.1016/j.ceb.2006.09.002. PubMed PMID: 17045790.

761 9. Di-Gregorio A, Sancho M, Stuckey DW, Crompton LA, Godwin J, Mishina Y, et al. BMP signalling inhibits
762 premature neural differentiation in the mouse embryo. Development. 2007;134(18):3359-69. PubMed PMID:
763 17699604.

764 10. Ribisi S, Jr., Mariani FV, Aamar E, Lamb TM, Frank D, Harland RM. Ras-mediated FGF signaling is required
765 for the formation of posterior but not anterior neural tissue in Xenopus laevis. Developmental biology.
766 2000;227(1):183-96.

767 11. Tzouanacou E, Wegener A, Wymeersch FJ, Wilson V, Nicolas JF. Redefining the progression of lineage
768 segregations during mammalian embryogenesis by clonal analysis. Developmental cell. 2009;17(3):365-76. PubMed
769 PMID: 19758561.

770 12. Turner DA, Hayward PC, Baillie-Johnson P, Rue P, Broome R, Faunes F, et al. Wnt/beta-catenin and FGF
771 signalling direct the specification and maintenance of a neuromesodermal axial progenitor in ensembles of mouse

772 embryonic stem cells. Development. 2014;141(22):4243-53. Epub 2014/11/06. doi: 10.1242/dev.112979. PubMed
773 PMID: 25371361; PubMed Central PMCID: PMC4302903.

774 13. Gouti M, Tsakiridis A, Wymeersch FJ, Huang Y, Kleinjung J, Wilson V, et al. In vitro generation of
775 neuromesodermal progenitors reveals distinct roles for wnt signalling in the specification of spinal cord and paraxial
776 mesoderm identity. PLoS biology. 2014;12(8):e1001937. Epub 2014/08/27. doi: 10.1371/journal.pbio.1001937.
777 PubMed PMID: 25157815; PubMed Central PMCID: PMC4144800.

778 14. Garriock RJ, Chalamalasetty RB, Kennedy MW, Canizales LC, Lewandoski M, Yamaguchi TP. Lineage tracing
779 of neuromesodermal progenitors reveals novel Wnt-dependent roles in trunk progenitor cell maintenance and
780 differentiation. Development. 2015;142(9):1628-38. Epub 2015/04/30. doi: 10.1242/dev.111922. PubMed PMID:
781 25922526; PubMed Central PMCID: PMC4419273.

782 15. Wymeersch FJ, Huang Y, Blin G, Cambray N, Wilkie R, Wong FC, et al. Position-dependent plasticity of
783 distinct progenitor types in the primitive streak. Elife. 2016;5:e10042. doi: 10.7554/eLife.10042. PubMed PMID:
784 26780186; PubMed Central PMCID: PMC4798969.

785 16. Bertrand N, Medevielle F, Pituello F. FGF signalling controls the timing of Pax6 activation in the neural tube.
786 Development. 2000;127(22):4837-43.

787 17. Diez del Corral R, Breitkreuz DN, Storey KG. Onset of neuronal differentiation is regulated by paraxial
788 mesoderm and requires attenuation of FGF signalling. Development. 2002;129(7):1681-91. PubMed PMID:
789 11923204.

790 18. Diez del Corral R, Olivera-Martinez I, Goriely A, Gale E, Maden M, Storey K. Opposing FGF and retinoid
791 pathways control ventral neural pattern, neuronal differentiation, and segmentation during body axis extension.
792 Neuron. 2003;40(1):65-79. PubMed PMID: 14527434.

793 19. Sirbu IO, Duester G. Retinoic-acid signalling in node ectoderm and posterior neural plate directs left-right
794 patterning of somitic mesoderm. Nature cell biology. 2006;8(3):271-7. doi: 10.1038/ncb1374. PubMed PMID:
795 16489341; PubMed Central PMCID: PMC2805411.

796 20. Kumar S, Duester G. Retinoic acid controls body axis extension by directly repressing Fgf8 transcription.
797 Development. 2014;141(15):2972-7. doi: 10.1242/dev.112367. PubMed PMID: 25053430; PubMed Central PMCID:
798 PMC4197666.

799 21. Wilson V, Olivera-Martinez I, Storey KG. Stem cells, signals and vertebrate body axis extension.
800 Development. 2009;136(10):1591-604. Epub 2009/04/28. doi: 10.1242/dev.021246. PubMed PMID: 19395637.

801 22. Lunn JS, Fishwick KJ, Halley PA, Storey KG. A spatial and temporal map of FGF/Erk1/2 activity and response
802 repertoires in the early chick embryo. Developmental biology. 2007;302(2):536-52. PubMed PMID: 17123506.

803 23. Corson LB, Yamanaka Y, Lai KM, Rossant J. Spatial and temporal patterns of ERK signaling during mouse
804 embryogenesis. Development. 2003;130(19):4527-37. PubMed PMID: 12925581.

805 24. Burdon T, Chambers I, Stracey C, Niwa H, Smith A. Signaling mechanisms regulating self-renewal and
806 differentiation of pluripotent embryonic stem cells. Cells Tissues Organs. 1999;165(3-4):131-43. PubMed PMID:
807 10592385.

808 25. Ying QL, Wray J, Nichols J, Batlle-Morera L, Doble B, Woodgett J, et al. The ground state of embryonic stem
809 cell self-renewal. Nature. 2008;453(7194):519-23. PubMed PMID: 18497825.

810 26. Ying QL, Stavridis M, Griffiths D, Li M, Smith A. Conversion of embryonic stem cells into neuroectodermal
811 precursors in adherent monoculture. Nature biotechnology. 2003;21(2):183-6. PubMed PMID: 12524553.

812 27. Stavridis MP, Lunn JS, Collins BJ, Storey KG. A discrete period of FGF-induced Erk1/2 signalling is required
813 for vertebrate neural specification. Development. 2007;134(16):2889-94. PubMed PMID: 17660197.

814 28. Kunath T, Saba-El-Leil MK, Almousailleakh M, Wray J, Meloche S, Smith A. FGF stimulation of the Erk1/2
815 signalling cascade triggers transition of pluripotent embryonic stem cells from self-renewal to lineage commitment.
816 Development. 2007;134(16):2895-902. PubMed PMID: 17660198.

817 29. Hamilton WB, Brickman JM. Erk signaling suppresses embryonic stem cell self-renewal to specify
818 endoderm. Cell reports. 2014;9(6):2056-70. Epub 2014/12/24. doi: 10.1016/j.celrep.2014.11.032. PubMed PMID:
819 25533345.

820 30. Greber B, Coulon P, Zhang M, Moritz S, Frank S, Muller-Molina AJ, et al. FGF signalling inhibits neural
821 induction in human embryonic stem cells. The EMBO journal. 2011;30(24):4874-84. Epub 2011/11/17. doi:
822 10.1038/emboj.2011.407. PubMed PMID: 22085933; PubMed Central PMCID: PMC3243624.

823 31. Stavridis MP, Collins BJ, Storey KG. Retinoic acid orchestrates fibroblast growth factor signalling to drive
824 embryonic stem cell differentiation. Development. 2010;137(6):881-90. Epub 2010/02/25. doi:
825 10.1242/dev.043117. PubMed PMID: 20179094; PubMed Central PMCID: PMCPMC2834455.

826 32. Greber B, Wu G, Bernemann C, Joo JY, Han DW, Ko K, et al. Conserved and divergent roles of FGF signaling
827 in mouse epiblast stem cells and human embryonic stem cells. Cell stem cell. 2010;6(3):215-26. Epub 2010/03/09.
828 doi: 10.1016/j.stem.2010.01.003. PubMed PMID: 20207225.

829 33. Patel NS, Rhinn M, Semprich CI, Halley PA, Dolle P, Bickmore WA, et al. FGF signalling regulates chromatin
830 organisation during neural differentiation via mechanisms that can be uncoupled from transcription. PLoS genetics.
831 2013;9(7):e1003614. Epub 2013/07/23. doi: 10.1371/journal.pgen.1003614. PubMed PMID: 23874217; PubMed
832 Central PMCID: PMC3715432.

833 34. Bernstein BE, Mikkelsen TS, Xie X, Kamal M, Huebert DJ, Cuff J, et al. A bivalent chromatin structure marks
834 key developmental genes in embryonic stem cells. Cell. 2006;125(2):315-26. Epub 2006/04/25. doi:
835 10.1016/j.cell.2006.02.041. PubMed PMID: 16630819.

836 35. Boyer LA, Plath K, Zeitlinger J, Brambrink T, Medeiros LA, Lee TI, et al. Polycomb complexes repress
837 developmental regulators in murine embryonic stem cells. Nature. 2006;441(7091):349-53. Epub 2006/04/21. doi:
838 10.1038/nature04733. PubMed PMID: 16625203.

839 36. Bracken AP, Dietrich N, Pasini D, Hansen KH, Helin K. Genome-wide mapping of Polycomb target genes
840 unravels their roles in cell fate transitions. Genes & development. 2006;20(9):1123-36. Epub 2006/04/19. doi:
841 10.1101/gad.381706. PubMed PMID: 16618801; PubMed Central PMCID: PMC1472472.

842 37. Lee TI, Jenner RG, Boyer LA, Guenther MG, Levine SS, Kumar RM, et al. Control of developmental regulators
843 by Polycomb in human embryonic stem cells. Cell. 2006;125(2):301-13. Epub 2006/04/25. doi:
844 10.1016/j.cell.2006.02.043. PubMed PMID: 16630818.

845 38. Mikkelsen TS, Ku M, Jaffe DB, Issac B, Lieberman E, Giannoukos G, et al. Genome-wide maps of chromatin
846 state in pluripotent and lineage-committed cells. Nature. 2007;448(7153):553-60. Epub 2007/07/03. doi:
847 10.1038/nature06008. PubMed PMID: 17603471; PubMed Central PMCID: PMC2921165.

848 39. Zhao XD, Han X, Chew JL, Liu J, Chiu KP, Choo A, et al. Whole-genome mapping of histone H3 Lys4 and 27
849 trimethylations reveals distinct genomic compartments in human embryonic stem cells. Cell stem cell.
850 2007;1(3):286-98. doi: 10.1016/j.stem.2007.08.004. PubMed PMID: 18371363.

851 40. Ferrai C, Torlai Triglia E, Risner-Janiczek JR, Rito T, Rackham OJ, de Santiago I, et al. RNA polymerase II
852 primes Polycomb-repressed developmental genes throughout terminal neuronal differentiation. Mol Syst Biol.
853 2017;13(10):946. Epub 2017/10/19. doi: 10.15252/msb.20177754. PubMed PMID: 29038337; PubMed Central
854 PMCID: PMCPMC5658700.

855 41. Di Croce L, Helin K. Transcriptional regulation by Polycomb group proteins. Nature structural & molecular
856 biology. 2013;20(10):1147-55. doi: 10.1038/nsmb.2669. PubMed PMID: 24096405.

857 42. Cao R, Wang L, Wang H, Xia L, Erdjument-Bromage H, Tempst P, et al. Role of histone H3 lysine 27
858 methylation in Polycomb-group silencing. Science. 2002;298(5595):1039-43. doi: 10.1126/science.1076997.
859 PubMed PMID: 12351676.

860 43. Czermin B, Melfi R, McCabe D, Seitz V, Imhof A, Pirrotta V. Drosophila enhancer of Zeste/ESC complexes
861 have a histone H3 methyltransferase activity that marks chromosomal Polycomb sites. Cell. 2002;111(2):185-96.
862 PubMed PMID: 12408863.

863 44. Kuzmichev A, Nishioka K, Erdjument-Bromage H, Tempst P, Reinberg D. Histone methyltransferase activity
864 associated with a human multiprotein complex containing the Enhancer of Zeste protein. Genes & development.

865 2002;16(22):2893-905. doi: 10.1101/gad.1035902. PubMed PMID: 12435631; PubMed Central PMCID:
866 PMC187479.

867 45. Margueron R, Reinberg D. The Polycomb complex PRC2 and its mark in life. Nature. 2011;469(7330):343-
868 9. doi: 10.1038/nature09784. PubMed PMID: 21248841; PubMed Central PMCID: PMC3760771.

869 46. Peng JC, Valouev A, Swigut T, Zhang J, Zhao Y, Sidow A, et al. Jarid2/Jumonji coordinates control of PRC2
870 enzymatic activity and target gene occupancy in pluripotent cells. Cell. 2009;139(7):1290-302. doi:
871 10.1016/j.cell.2009.12.002. PubMed PMID: 20064375; PubMed Central PMCID: PMC2911953.

872 47. Landeira D, Sauer S, Poot R, Dvorkina M, Mazzarella L, Jorgensen HF, et al. Jarid2 is a PRC2 component in
873 embryonic stem cells required for multi-lineage differentiation and recruitment of PRC1 and RNA Polymerase II to
874 developmental regulators. Nature cell biology. 2010;12(6):618-24. Epub 2010/05/18. doi: 10.1038/ncb2065.
875 PubMed PMID: 20473294.

876 48. Pasini D, Cloos PA, Walfridsson J, Olsson L, Bukowski JP, Johansen JV, et al. JARID2 regulates binding of the
877 Polycomb repressive complex 2 to target genes in ES cells. Nature. 2010;464(7286):306-10. Epub 2010/01/16. doi:
878 10.1038/nature08788. PubMed PMID: 20075857.

879 49. Sanulli S, Justin N, Teissandier A, Ancelin K, Portoso M, Caron M, et al. Jarid2 Methylation via the PRC2
880 Complex Regulates H3K27me3 Deposition during Cell Differentiation. Molecular cell. 2015;57(5):769-83. Epub
881 2015/01/27. doi: 10.1016/j.molcel.2014.12.020. PubMed PMID: 25620564; PubMed Central PMCID:
882 PMCPMC4352895.

883 50. Cooper S, Grijzenhout A, Underwood E, Ancelin K, Zhang T, Nesterova TB, et al. Jarid2 binds mono-
884 ubiquitylated H2A lysine 119 to mediate crosstalk between Polycomb complexes PRC1 and PRC2. Nature
885 communications. 2016;7:13661. Epub 2016/11/29. doi: 10.1038/ncomms13661. PubMed PMID: 27892467;
886 PubMed Central PMCID: PMCPMC5133711.

887 51. Wang L, Brown JL, Cao R, Zhang Y, Kassis JA, Jones RS. Hierarchical recruitment of polycomb group silencing
888 complexes. Molecular cell. 2004;14(5):637-46. doi: 10.1016/j.molcel.2004.05.009. PubMed PMID: 15175158.

889 52. Wang H, Wang L, Erdjument-Bromage H, Vidal M, Tempst P, Jones RS, et al. Role of histone H2A
890 ubiquitination in Polycomb silencing. Nature. 2004;431(7010):873-8. doi: 10.1038/nature02985. PubMed PMID:
891 15386022.

892 53. Zhou W, Zhu P, Wang J, Pascual G, Ohgi KA, Lozach J, et al. Histone H2A monoubiquitination represses
893 transcription by inhibiting RNA polymerase II transcriptional elongation. Molecular cell. 2008;29(1):69-80. Epub
894 2008/01/22. doi: 10.1016/j.molcel.2007.11.002. PubMed PMID: 18206970; PubMed Central PMCID: PMC2327256.

895 54. Muller J, Verrijzer P. Biochemical mechanisms of gene regulation by polycomb group protein complexes.
896 Current opinion in genetics & development. 2009;19(2):150-8. doi: 10.1016/j.gde.2009.03.001. PubMed PMID:
897 19345089.

898 55. Marks H, Kalkan T, Menafra R, Denissov S, Jones K, Hofemeister H, et al. The transcriptional and epigenomic
899 foundations of ground state pluripotency. Cell. 2012;149(3):590-604. doi: 10.1016/j.cell.2012.03.026. PubMed
900 PMID: 22541430; PubMed Central PMCID: PMC3398752.

901 56. Tee WW, Shen SS, Oksuz O, Narendra V, Reinberg D. Erk1/2 activity promotes chromatin features and
902 RNAPII phosphorylation at developmental promoters in mouse ESCs. Cell. 2014;156(4):678-90. Epub 2014/02/18.
903 doi: 10.1016/j.cell.2014.01.009. PubMed PMID: 24529373; PubMed Central PMCID: PMC4006806.

904 57. van Mierlo G, Dirks RAM, De Clerck L, Brinkman AB, Huth M, Kloet SL, et al. Integrative Proteomic Profiling
905 Reveals PRC2-Dependent Epigenetic Crosstalk Maintains Ground-State Pluripotency. Cell stem cell. 2019;24(1):123-
906 37 e8. Epub 2018/11/26. doi: 10.1016/j.stem.2018.10.017. PubMed PMID: 30472157.

907 58. Goke J, Chan YS, Yan J, Vingron M, Ng HH. Genome-wide kinase-chromatin interactions reveal the
908 regulatory network of ERK signaling in human embryonic stem cells. Molecular cell. 2013;50(6):844-55. Epub
909 2013/06/04. doi: 10.1016/j.molcel.2013.04.030. PubMed PMID: 23727019.

910 59. Gerard M, Zakany J, Duboule D. Interspecies exchange of a Hoxd enhancer in vivo induces premature
911 transcription and anterior shift of the sacrum. Developmental biology. 1997;190(1):32-40. doi:
912 10.1006/dbio.1997.8679. PubMed PMID: 9331329.

913 60. Woo CJ, Kharchenko PV, Daheron L, Park PJ, Kingston RE. A region of the human HOXD cluster that confers
914 polycomb-group responsiveness. Cell. 2010;140(1):99-110. doi: 10.1016/j.cell.2009.12.022. PubMed PMID:
915 20085705; PubMed Central PMCID: PMC3324942.

916 61. Leeb M, Pasini D, Novatchkova M, Jaritz M, Helin K, Wutz A. Polycomb complexes act redundantly to
917 repress genomic repeats and genes. Genes & development. 2010;24(3):265-76. doi: 10.1101/gad.544410. PubMed
918 PMID: 20123906; PubMed Central PMCID: PMC2811828.

919 62. Soshnikova N, Duboule D. Epigenetic temporal control of mouse Hox genes in vivo. Science.
920 2009;324(5932):1320-3. Epub 2009/06/06. doi: 10.1126/science.1171468. PubMed PMID: 19498168.

921 63. Huang D, Chen SW, Langston AW, Gudas LJ. A conserved retinoic acid responsive element in the murine
922 Hoxb-1 gene is required for expression in the developing gut. Development. 1998;125(16):3235-46. Epub
923 1998/07/22. PubMed PMID: 9671595.

924 64. Verrier L, Davidson L, Gierlinski M, Dady A, Storey KG. Neural differentiation, selection and transcriptomic
925 profiling of human neuromesodermal progenitor-like cells in vitro. Development. 2018;145(16). Epub 2018/06/15.
926 doi: 10.1242/dev.166215. PubMed PMID: 29899136; PubMed Central PMCID: PMCPMC6124542.

927 65. Buenrostro JD, Giresi PG, Zaba LC, Chang HY, Greenleaf WJ. Transposition of native chromatin for fast and
928 sensitive epigenomic profiling of open chromatin, DNA-binding proteins and nucleosome position. Nature methods.
929 2013;10(12):1213-8. doi: 10.1038/nmeth.2688. PubMed PMID: 24097267; PubMed Central PMCID: PMC3959825.

930 66. Visel A, Minovitsky S, Dubchak I, Pennacchio LA. VISTA Enhancer Browser--a database of tissue-specific
931 human enhancers. Nucleic acids research. 2007;35(Database issue):D88-92. Epub 2006/11/30. doi:
932 10.1093/nar/gkl822. PubMed PMID: 17130149; PubMed Central PMCID: PMCPMC1716724.

933 67. Sloan CA, Chan ET, Davidson JM, Malladi VS, Strattan JS, Hitz BC, et al. ENCODE data at the ENCODE portal.
934 Nucleic acids research. 2016;44(D1):D726-32. Epub 2015/11/04. doi: 10.1093/nar/gkv1160. PubMed PMID:
935 26527727; PubMed Central PMCID: PMCPMC4702836.

936 68. Eskeland R, Leeb M, Grimes GR, Kress C, Boyle S, Sproul D, et al. Ring1B compacts chromatin structure and
937 represses gene expression independent of histone ubiquitination. Molecular cell. 2010;38(3):452-64. Epub
938 2010/05/18. doi: 10.1016/j.molcel.2010.02.032. PubMed PMID: 20471950; PubMed Central PMCID: PMC3132514.

939 69. Montgomery ND, Yee D, Chen A, Kalantry S, Chamberlain SJ, Otte AP, et al. The murine polycomb group
940 protein Eed is required for global histone H3 lysine-27 methylation. Current biology : CB. 2005;15(10):942-7. doi:
941 10.1016/j.cub.2005.04.051. PubMed PMID: 15916951.

942 70. Morey L, Pascual G, Cozzuto L, Roma G, Wutz A, Benitah SA, et al. Nonoverlapping functions of the
943 Polycomb group Cbx family of proteins in embryonic stem cells. Cell stem cell. 2012;10(1):47-62. doi:
944 10.1016/j.stem.2011.12.006. PubMed PMID: 22226355.

945 71. Eskeland R, Freyer E, Leeb M, Wutz A, Bickmore WA. Histone acetylation and the maintenance of
946 chromatin compaction by Polycomb repressive complexes. Cold Spring Harbor symposia on quantitative biology.
947 2010;75:71-8. Epub 2011/04/20. doi: 10.1101/sqb.2010.75.053. PubMed PMID: 21502416.

948 72. Kundu S, Ji F, Sunwoo H, Jain G, Lee JT, Sadreyev RI, et al. Polycomb Repressive Complex 1 Generates
949 Discrete Compacted Domains that Change during Differentiation. Molecular cell. 2017;65(3):432-46 e5. Epub
950 2017/02/06. doi: 10.1016/j.molcel.2017.01.009. PubMed PMID: 28157505; PubMed Central PMCID:
951 PMCPMC5421375.

952 73. Brookes E, Pombo A. Modifications of RNA polymerase II are pivotal in regulating gene expression states.
953 EMBO reports. 2009;10(11):1213-9. Epub 2009/10/17. doi: 10.1038/embor.2009.221. PubMed PMID: 19834511;
954 PubMed Central PMCID: PMCPMC2775184.

955 74. Kadoch C, Williams RT, Calarco JP, Miller EL, Weber CM, Braun SM, et al. Dynamics of BAF-Polycomb
956 complex opposition on heterochromatin in normal and oncogenic states. Nature genetics. 2017;49(2):213-22. Epub
957 2016/12/13. doi: 10.1038/ng.3734. PubMed PMID: 27941796; PubMed Central PMCID: PMCPMC5285326.

958 75. Lessard J, Wu JI, Ranish JA, Wan M, Winslow MM, Staahl BT, et al. An essential switch in subunit
959 composition of a chromatin remodeling complex during neural development. Neuron. 2007;55(2):201-15. doi:
960 10.1016/j.neuron.2007.06.019. PubMed PMID: 17640523; PubMed Central PMCID: PMC2674110.

961 76. Staahl BT, Crabtree GR. Creating a neural specific chromatin landscape by npBAF and nBAF complexes.
962 Curr Opin Neurobiol. 2013;23(6):903-13. Epub 2013/10/05. doi: 10.1016/j.conb.2013.09.003. PubMed PMID:
963 24090879; PubMed Central PMCID: PMCPMC3878911.

964 77. Olivera-Martinez I, Schurch N, Li RA, Song J, Halley PA, Das RM, et al. Major transcriptome re-organisation
965 and abrupt changes in signalling, cell cycle and chromatin regulation at neural differentiation in vivo. Development.
966 2014;141(16):3266-76. Epub 2014/07/27. doi: 10.1242/dev.112623. PubMed PMID: 25063452.

967 78. Nichols J, Smith A. Naive and primed pluripotent states. Cell stem cell. 2009;4(6):487-92. Epub 2009/06/06.
968 doi: 10.1016/j.stem.2009.05.015. PubMed PMID: 19497275.

969 79. Silva J, Barrandon O, Nichols J, Kawaguchi J, Theunissen TW, Smith A. Promotion of reprogramming to
970 ground state pluripotency by signal inhibition. PLoS biology. 2008;6(10):e253. Epub 2008/10/24. doi:
971 10.1371/journal.pbio.0060253. PubMed PMID: 18942890; PubMed Central PMCID: PMCPMC2570424.

972 80. Nett IR, Mulas C, Gatto L, Lilley KS, Smith A. Negative feedback via RSK modulates Erk-dependent
973 progression from naive pluripotency. EMBO reports. 2018;19(8). Epub 2018/06/14. doi:
974 10.15252/embr.201745642. PubMed PMID: 29895711; PubMed Central PMCID: PMCPMC6073214.

975 81. Sterneckert J, Stehling M, Bernemann C, Arauzo-Bravo MJ, Greber B, Gentile L, et al. Neural induction
976 intermediates exhibit distinct roles of Fgf signaling. Stem cells. 2010;28(10):1772-81. Epub 2010/08/18. doi:
977 10.1002/stem.498. PubMed PMID: 20715182.

978 82. Azuara V, Perry P, Sauer S, Spivakov M, Jorgensen HF, John RM, et al. Chromatin signatures of pluripotent
979 cell lines. Nature cell biology. 2006;8(5):532-8. Epub 2006/03/30. doi: 10.1038/ncb1403. PubMed PMID: 16570078.

980 83. Stock JK, Giadrossi S, Casanova M, Brookes E, Vidal M, Koseki H, et al. Ring1-mediated ubiquitination of
981 H2A restrains poised RNA polymerase II at bivalent genes in mouse ES cells. Nature cell biology. 2007;9(12):1428-
982 35. Epub 2007/11/27. doi: 10.1038/ncb1663. PubMed PMID: 18037880.

983 84. Brookes E, de Santiago I, Hebenstreit D, Morris KJ, Carroll T, Xie SQ, et al. Polycomb associates genome-
984 wide with a specific RNA polymerase II variant, and regulates metabolic genes in ESCs. Cell stem cell.
985 2012;10(2):157-70. doi: 10.1016/j.stem.2011.12.017. PubMed PMID: 22305566.

986 85. Weiner A, Lara-Astiaso D, Krupalnik V, Gafni O, David E, Winter DR, et al. Co-ChIP enables genome-wide
987 mapping of histone mark co-occurrence at single-molecule resolution. Nature biotechnology. 2016;34(9):953-61.
988 Epub 2016/07/28. doi: 10.1038/nbt.3652. PubMed PMID: 27454738.

989 86. Cruz-Molina S, Respuela P, Tebartz C, Kolovos P, Nikolic M, Fueyo R, et al. PRC2 Facilitates the Regulatory
990 Topology Required for Poised Enhancer Function during Pluripotent Stem Cell Differentiation. Cell stem cell.
991 2017;20(5):689-705 e9. Epub 2017/03/14. doi: 10.1016/j.stem.2017.02.004. PubMed PMID: 28285903.

992 87. Fallon JF, Lopez A, Ros MA, Savage MP, Olwin BB, Simandl BK. FGF-2: apical ectodermal ridge growth signal
993 for chick limb development. Science. 1994;264(5155):104-7.

994 88. Sun X, Mariani FV, Martin GR. Functions of FGF signalling from the apical ectodermal ridge in limb
995 development. Nature. 2002;418(6897):501-8. Epub 2002/08/02. doi: 10.1038/nature00902. PubMed PMID:
996 12152071.

997 89. Min H, Danilenko DM, Scully SA, Bolon B, Ring BD, Tarpley JE, et al. Fgf-10 is required for both limb and
998 lung development and exhibits striking functional similarity to Drosophila branchless. Genes & development.
999 1998;12(20):3156-61.

1000 90. Kettunen P, Thesleff I. Expression and function of FGFs-4, -8, and -9 suggest functional redundancy and
1001 repetitive use as epithelial signals during tooth morphogenesis. Developmental dynamics : an official publication of
1002 the American Association of Anatomists. 1998;211(3):256-68.

1003 91. Crossley PH, Martinez S, Martin GR. Midbrain development induced by FGF8 in the chick embryo. Nature.
1004 1996;380(6569):66-8.

1005 92. Mishra A, Oules B, Pisco AO, Ly T, Liakath-Ali K, Walko G, et al. A protein phosphatase network controls the
1006 temporal and spatial dynamics of differentiation commitment in human epidermis. Elife. 2017;6. Epub 2017/10/19.
1007 doi: 10.7554/eLife.27356. PubMed PMID: 29043977; PubMed Central PMCID: PMCPMC5667932.

1008 93. Dale JK, Malapert P, Chal J, Vilhais-Neto G, Maroto M, Johnson T, et al. Oscillations of the snail genes in the
1009 presomitic mesoderm coordinate segmental patterning and morphogenesis in vertebrate somitogenesis.
1010 Developmental cell. 2006;10(3):355-66. Epub 2006/03/07. doi: 10.1016/j.devcel.2006.02.011. PubMed PMID:
1011 16516838.

1012 94. Allan C, Burel JM, Moore J, Blackburn C, Linkert M, Loynton S, et al. OMERO: flexible, model-driven data
1013 management for experimental biology. Nature methods. 2012;9(3):245-53. Epub 2012/03/01. doi:
1014 10.1038/nmeth.1896. PubMed PMID: 22373911; PubMed Central PMCID: PMCPMC3437820.

1015 95. Pfaffl MW. A new mathematical model for relative quantification in real-time RT-PCR. Nucleic acids
1016 research. 2001;29(9):e45. PubMed PMID: 11328886.

1017 96. Buenrostro JD, Wu B, Chang HY, Greenleaf WJ. ATAC-seq: A Method for Assaying Chromatin Accessibility
1018 Genome-Wide. Current protocols in molecular biology. 2015;109:21 9 1-9. doi: 10.1002/0471142727.mb2129s109.
1019 PubMed PMID: 25559105; PubMed Central PMCID: PMC4374986.

1020 97. Martin M. Cutadapt removes adapter sequences from high-throughput sequencing reads. .
1021 EMBnetjournal. 2011;17:10-2. doi: https://doi.org/10.14806/ej.17.1.200.

1022 98. Li H, Handsaker B, Wysoker A, Fennell T, Ruan J, Homer N, et al. The Sequence Alignment/Map format and
1023 SAMtools. Bioinformatics. 2009;25(16):2078-9. doi: 10.1093/bioinformatics/btp352. PubMed PMID: 19505943;
1024 PubMed Central PMCID: PMC2723002.

1025 99. Li H, Durbin R. Fast and accurate short read alignment with Burrows-Wheeler transform. Bioinformatics.
1026 2009;25(14):1754-60. doi: 10.1093/bioinformatics/btp324. PubMed PMID: 19451168; PubMed Central PMCID:
1027 PMC2705234.

1028 100. Karolchik D, Hinrichs AS, Furey TS, Roskin KM, Sugnet CW, Haussler D, et al. The UCSC Table Browser data
1029 retrieval tool. Nucleic acids research. 2004;32(Database issue):D493-6. doi: 10.1093/nar/gkh103. PubMed PMID:
1030 14681465; PubMed Central PMCID: PMC308837.

1031 101. Quinlan AR, Hall IM. BEDTools: a flexible suite of utilities for comparing genomic features. Bioinformatics.
1032 2010;26(6):841-2. doi: 10.1093/bioinformatics/btq033. PubMed PMID: 20110278; PubMed Central PMCID:
1033 PMC2832824.

1034 102. Kent WJ, Zweig AS, Barber G, Hinrichs AS, Karolchik D. BigWig and BigBed: enabling browsing of large
1035 distributed datasets. Bioinformatics. 2010;26(17):2204-7. doi: 10.1093/bioinformatics/btq351. PubMed PMID:
1036 20639541; PubMed Central PMCID: PMC2922891.

1037 103. Zhang Y, Liu T, Meyer CA, Eeckhoute J, Johnson DS, Bernstein BE, et al. Model-based analysis of ChIP-Seq
1038 (MACS). Genome Biol. 2008;9(9):R137. doi: 10.1186/gb-2008-9-9-r137. PubMed PMID: 18798982; PubMed Central
1039 PMCID: PMC2592715.

1040 104. Shen L, Shao NY, Liu X, Maze I, Feng J, Nestler EJ. diffReps: detecting differential chromatin modification
1041 sites from ChIP-seq data with biological replicates. PloS one. 2013;8(6):e65598. doi:
1042 10.1371/journal.pone.0065598. PubMed PMID: 23762400; PubMed Central PMCID: PMC3677880.

1043 105. Heinz S, Benner C, Spann N, Bertolino E, Lin YC, Laslo P, et al. Simple combinations of lineage-determining
1044 transcription factors prime cis-regulatory elements required for macrophage and B cell identities. Molecular cell.
1045 2010;38(4):576-89. doi: 10.1016/j.molcel.2010.05.004. PubMed PMID: 20513432; PubMed Central PMCID:
1046 PMC2898526.

1047 106. Ramirez F, Ryan DP, Gruning B, Bhardwaj V, Kilpert F, Richter AS, et al. deepTools2: a next generation web
1048 server for deep-sequencing data analysis. Nucleic acids research. 2016;44(W1):W160-5. Epub 2016/04/16. doi:
1049 10.1093/nar/gkw257. PubMed PMID: 27079975; PubMed Central PMCID: PMCPMC4987876.

1050

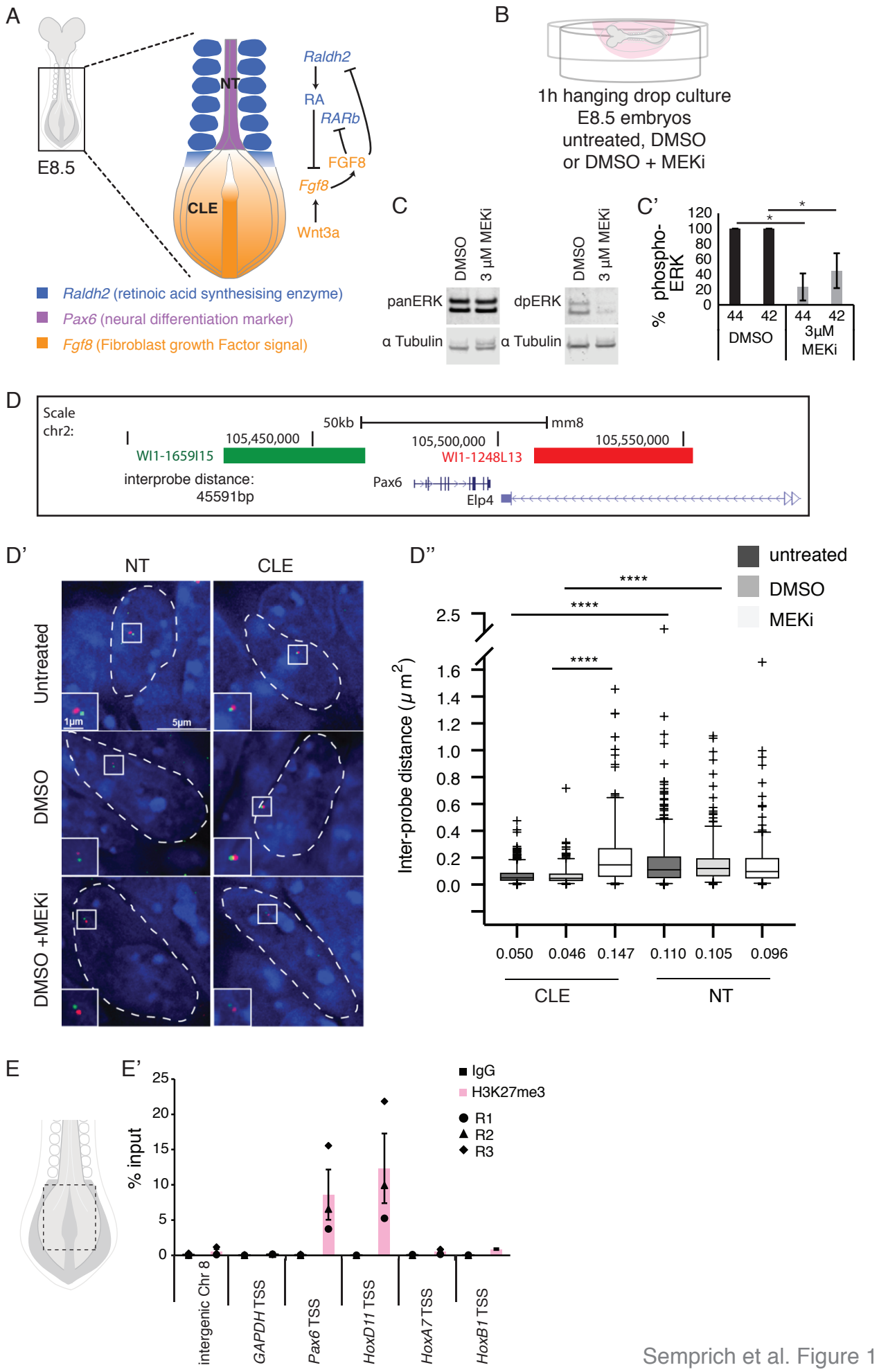

Semprich et al. Figure 1

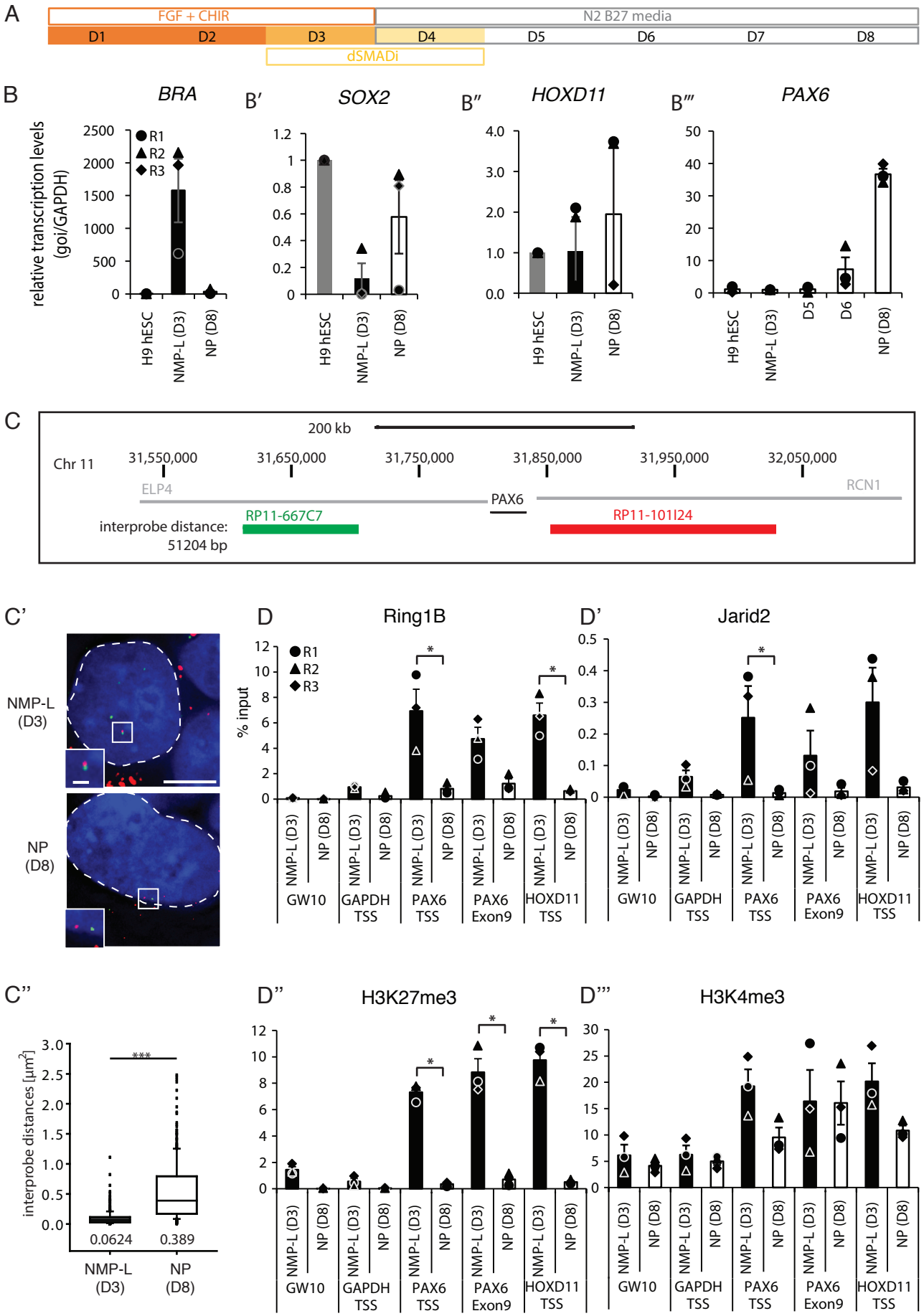

Semprich et al. Figure 2

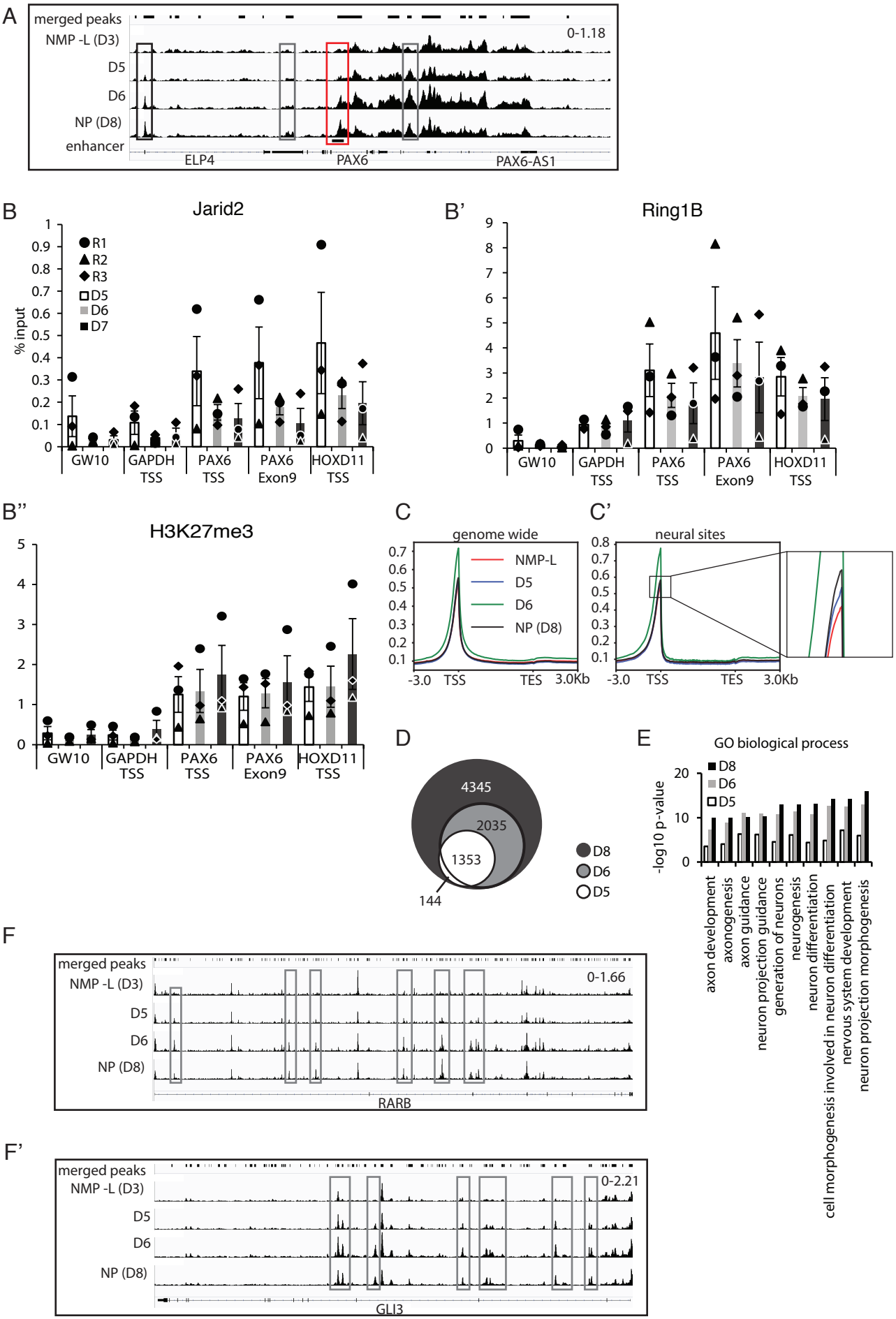

Semprich et al. Figure 3

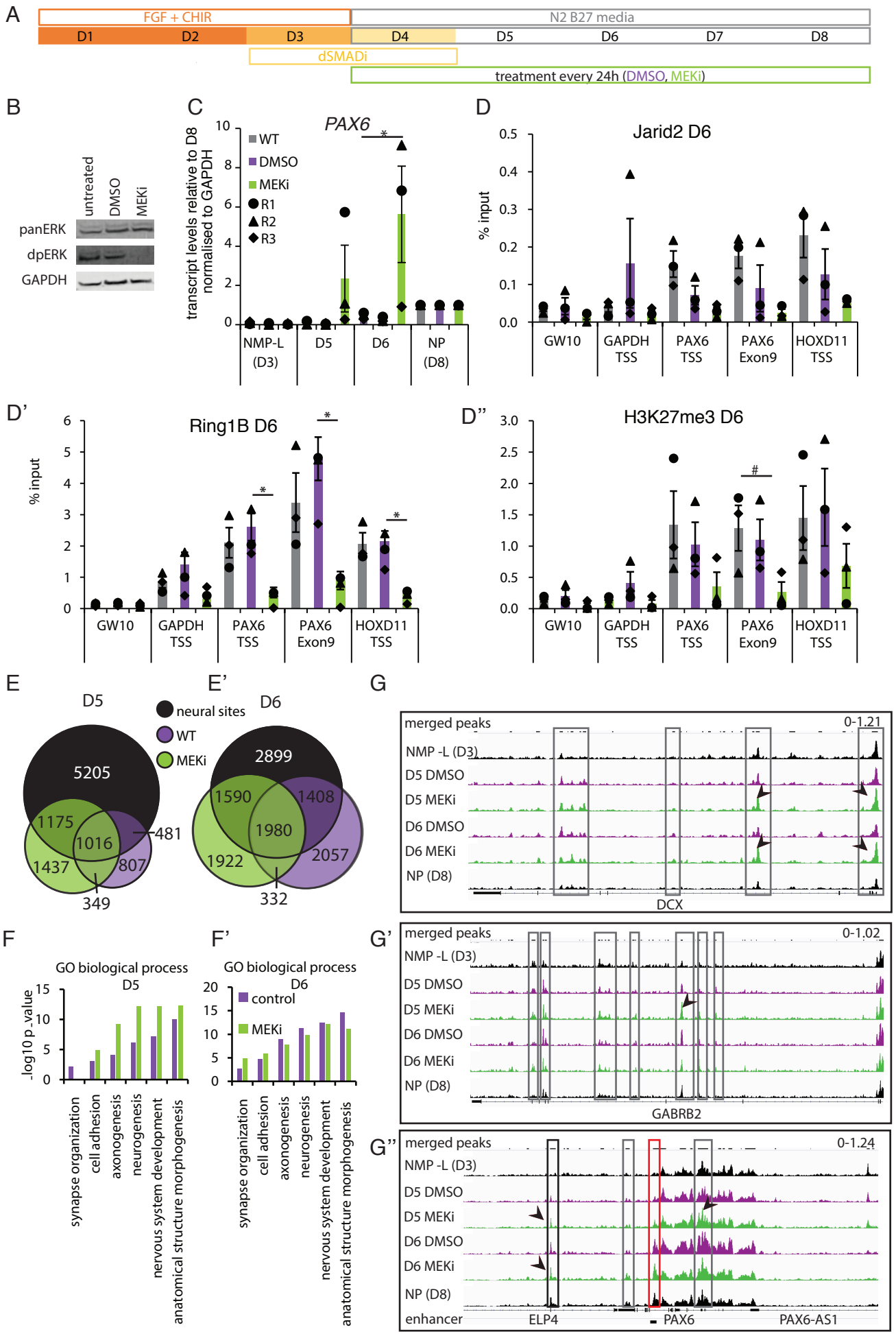

Semprich et al. Figure 4

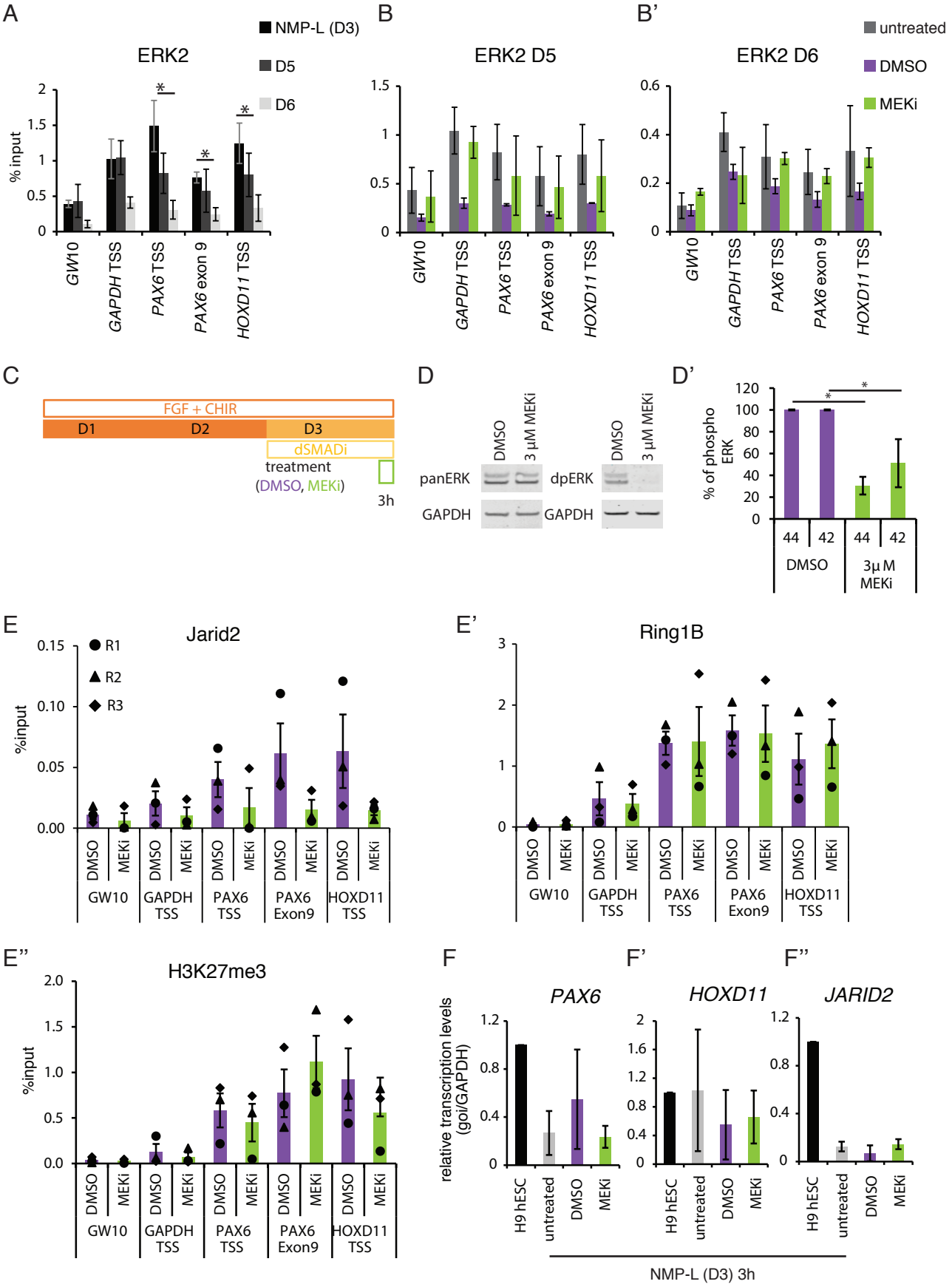

Semprich et al. Figure 5

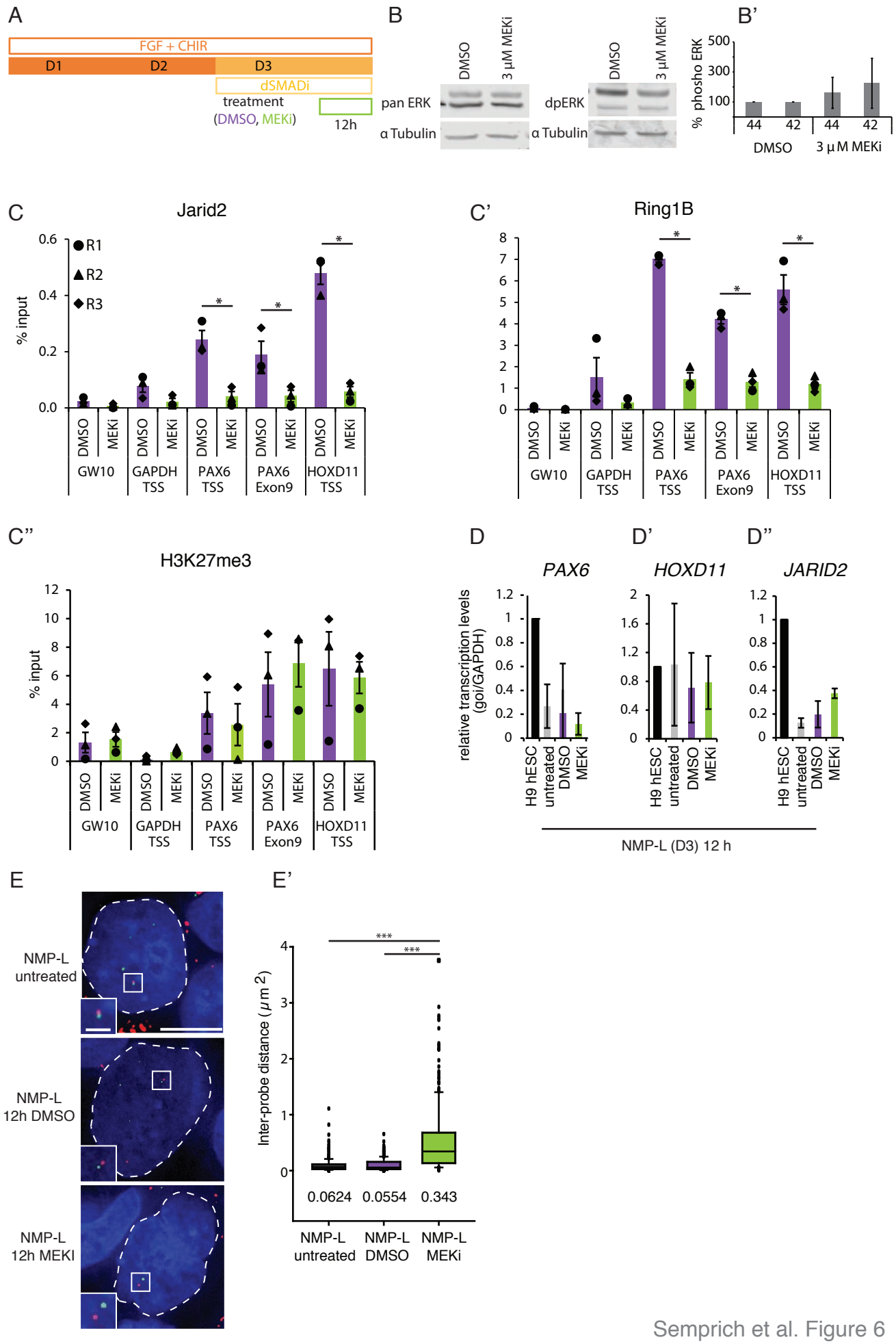

Semprich et al. Figure 6

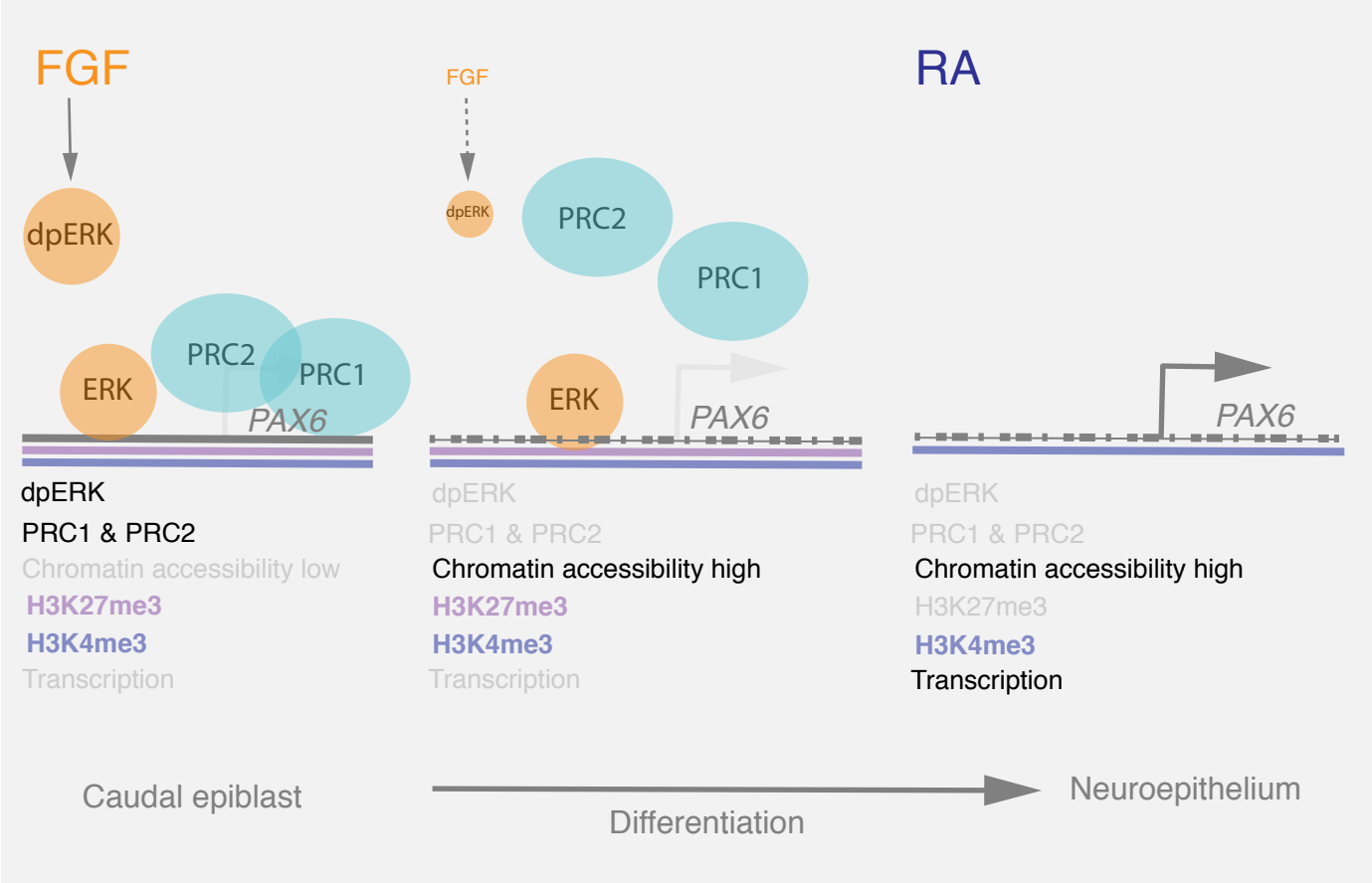

Semprich et al Figure 7

Supplementary Figure and Table legends

Figure S1 Neural sites identified by ATAC-seq overlap with known active enhancer sites in human embryonic neural tissue and *in vitro* generated neural progenitors. Comparison of peaks called from publicly available ChIPseq data sets for H3K9me3, H3K27me3, H3K4me1 and H3K27ac from the ENCODE regulatory element database (Sloan et al., 2016) with neural sites from Figure 3 show high proportion of overlap for active enhancer marks H3K4me1 and H3K27ac in neural embryonic tissue (brain and spinal cord) and *in vitro* generated neural progenitors. Data sets from embryonic lung thymus and kidney tissues were used as controls and showed smaller proportions of overlap. Furthermore H3K9me3 and H3K27me3 were used as control for repressive chromatin modification, H3K9me3 especially is known to be enriched in heterochromatin (Becker et al., 2016) and shows little to no overlap with the neural sites.

Figure S2 MEKi treatment does not alter PRC protein occupancy on day 5 ChIP-qPCR for Jarid2 and Ring1B for untreated, DMSO and MEKI treated cells during differentiation from NMP-L (D3) to D5 (n = 3 independent experiments indicated with circles, triangles and diamonds, bar = average, error bars = SEM, * = $p \leq 0.05$ or t-test showed no significant difference);

Figure S3 NMP-L cells cultured for 12h in MEKi no longer exhibit reduced ERK phosphorylation, but have increased PKB phosphorylation levels (A and B) Western blot analysis of NMP-L (D3) protein extracts using phospho-specific antibodies against ERK1/2 and PKB alongside pan antibodies. (C and D) quantification of band intensity shows no reduction in ERK phosphorylation but increased levels of PKB phosphorylation (n = 3 independent experiments error bars = SEM, * = $p \leq 0.05$ or t-test showed no significant difference).

Table S1 Regions and associated genes opening during *in vitro* neural differentiation identified by ATACseq. During *in vitro* neural differentiation from NMP-L (D3) to NP (D8) 7877 regions open up associated with 4001 genes. Opening regions are defined by chromosomal position and associated gene names have been identified by proximity.

Table S2 List of genes associated with open chromatin regions at different time points during *in vitro* neural differentiation. During *in vitro* neural differentiation ATAC-seq reveals that an increasing number of neural genes appear that are associated with open chromatin (by proximity). By day 5 of differentiation, regions associated with 1143 genes have opened, by day 6 regions associated with 2137 genes are open and by final day 8 regions associated with 4001 genes are now more accessible.

Table S3 List of genes associated with open chromatin regions comparing control and MEK inhibition condition on day 5 and day 6 of the *in vitro* neural differentiation. ATAC-seq showed that during the *in vitro* neural differentiation treatment with the MEK inhibitor PD184352 results in an increase in open chromatin. By day 5 of differentiation 1143 genes are associated with these open regions, while in the presence of MEKi, 2537 genes are associated with opened chromatin regions, 612 of which are unique to D5 MEKi condition); on day 6, 2137 genes are associated with open chromatin and with MEKi treatment regions associated with 3283 genes are open, 2045 of which were not associated with open regions in the D6 control condition and 1584 genes are unique to D6 MEKi condition.

Table S4 Names, co-ordinates and size and interprobe distances of mouse fosmids and human BAC clones used.

Table S5 Antibodies and amounts used for chromatin immunoprecipitation

Table S6 Sequences of primers used for the quantification of transcript levels

Table S7 Primary and secondary antibodies used to detect proteins transferred onto a membrane after size separation on an SDS gel.

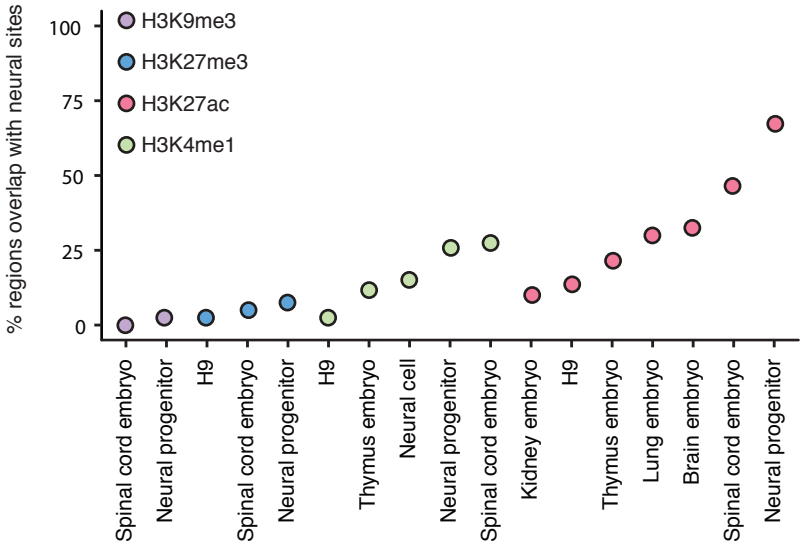

Semprich et al. Figure S1

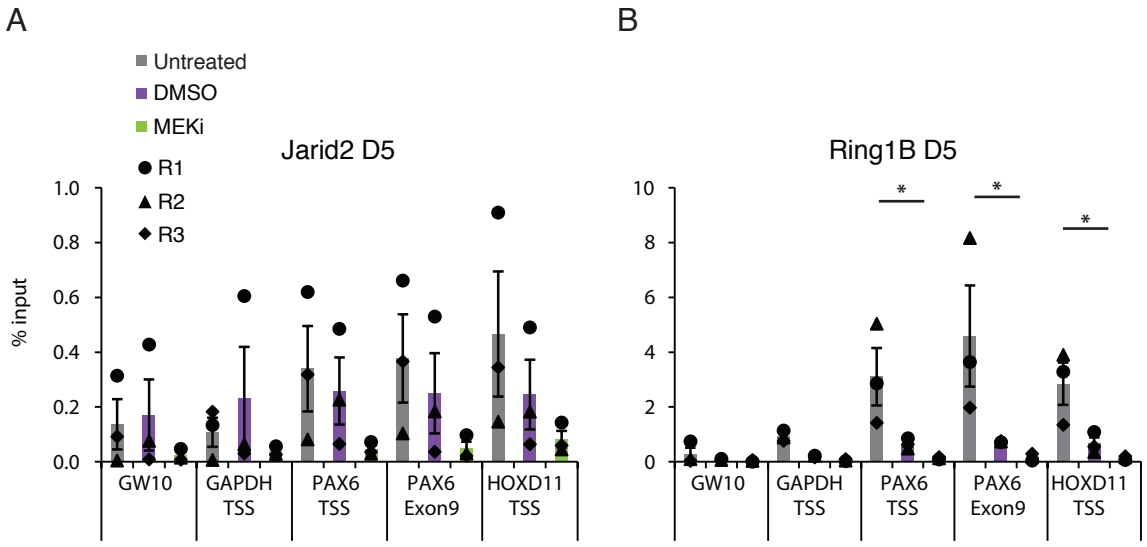

Semprich et al. Figure S2

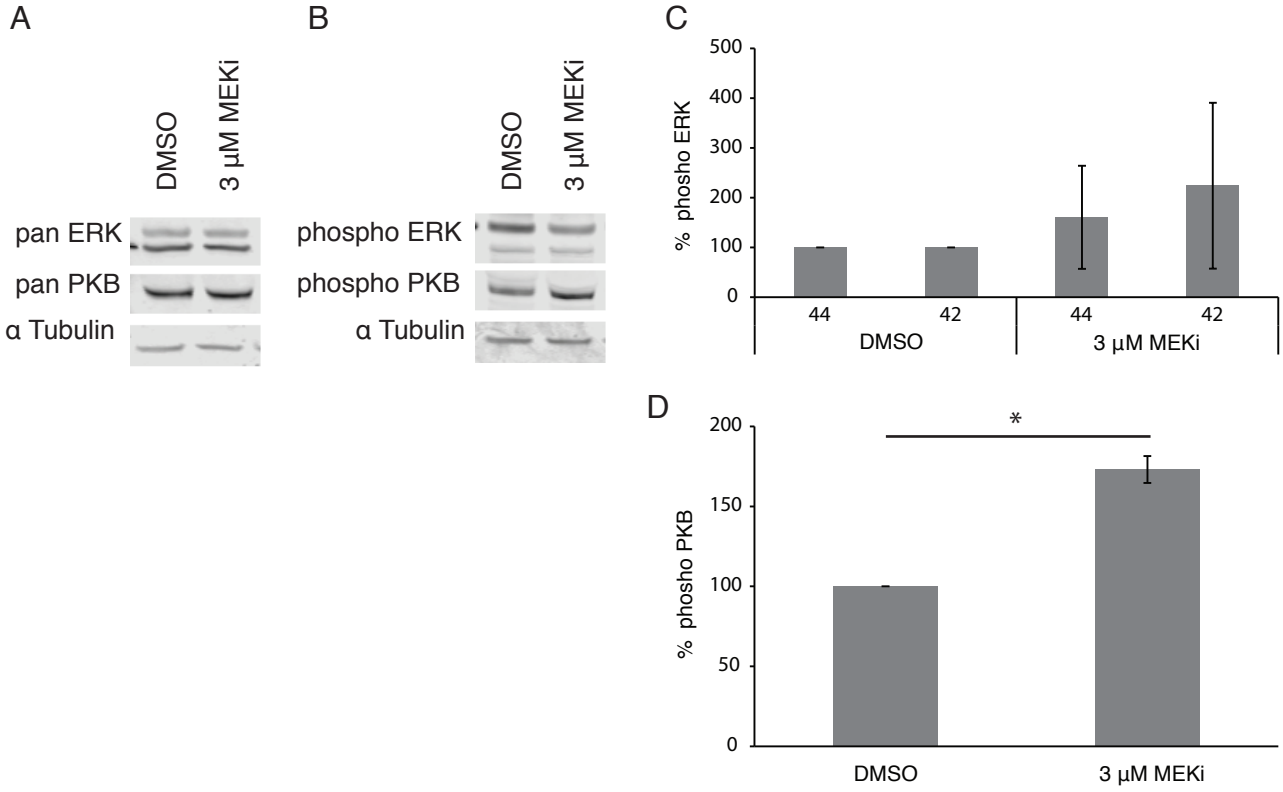

Semprich et al. Figure S3